Global Change Biology (2003) **9,** 1543–1566, doi: 10.1046/j.1529-8817.2003.00681.x

A dynamic global vegetation model for use with climate models: concepts and description of simulated vegetation dynamics

GORDON B. BONAN*, SAMUEL LEVIS*, STEPHEN SITCH†, MARIANA VERTENSTEIN* and KEITH W. OLESON*

**National Center for Atmospheric Research, PO Box 3000, Boulder, CO 80307, USA, †Potsdam Institut für Klimafolgenforschung (PIK) e.V., Telegrafenberg, PO Box 60 12 03, D-144 12 Potsdam, Germany*

Abstract

Changes in vegetation structure and biogeography due to climate change feedback to alter climate by changing fluxes of energy, moisture, and momentum between land and atmosphere. While the current class of land process models used with climate models parameterizes these fluxes in detail, these models prescribe surface vegetation and leaf area from data sets. In this paper, we describe an approach in which ecological concepts from a global vegetation dynamics model are added to the land component of a climate model to grow plants interactively. The vegetation dynamics model is the Lund–Potsdam–Jena (LPJ) dynamic global vegetation model. The land model is the National Center for Atmospheric Research (NCAR) Land Surface Model (LSM). Vegetation is defined in terms of plant functional types. Each plant functional type is represented by an individual plant with the average biomass, crown area, height, and stem diameter (trees only) of its population, by the number of individuals in the population, and by the fractional cover in the grid cell. Three time-scales (minutes, days, and years) govern the processes. Energy fluxes, the hydrologic cycle, and carbon assimilation, core processes in LSM, occur at a 20 min time step. Instantaneous net assimilated carbon is accumulated annually to update vegetation once a year. This is carried out with the addition of establishment, resource competition, growth, mortality, and fire parameterizations from LPJ. The leaf area index is updated daily based on prevailing environmental conditions, but the maximum value depends on the annual vegetation dynamics. The coupling approach is successful. The model simulates global biogeography, net primary production, and dynamics of tundra, boreal forest, northern hardwood forest, tropical rainforest, and savanna ecosystems, which are consistent with observations. This suggests that the model can be used with a climate model to study biogeophysical feedbacks in the climate system related to vegetation dynamics.

Keywords: biogeography, climate model, dynamic global vegetation model, vegetation dynamics

Received 22 February 2002; revised version received 3 December 2002 and accepted 16 June 2003

Introduction

Terrestrial ecosystems affect climate through fluxes of energy, water, momentum, CO_2, trace gases, and mineral aerosols. Changes in community composition and ecosystem structure alter these fluxes and in doing so, alter climate. Most studies of vegetation feedback on climate have focused on biogeophysical processes related to energy and water.

Vegetation feedback on climate is seen in North Africa, where the contrasts between barren and vegetated landscapes in albedo, surface roughness, surface conductance, and soil texture influence precipitation. Increased solar radiation 6000 years ago strengthened the summer monsoon (Kutzbach & Otto-Bliesner, 1982; Braconnot *et al.*, 2000), allowing grasses and shrubs to cover much of North Africa (Hoelzmann *et al.*, 1998; Jolly *et al.*, 1998a, b; Prentice *et al.*, 2000).

Correspondence: G. B. Bonan, National Center for Atmospheric Research, PO Box 3000, Boulder, CO 80307, USA, fax 303 497 1695, e-mail: bonan@ucar.edu

Climate simulations with prescribed vegetation show that this greening of the Sahara results in more precipitation (Kutzbach *et al*., 1996).

Another example is the boreal forest–tundra ecotone. Climate simulations in which the boreal forest is replaced with tundra or bare ground show that trees warm climate primarily by masking snow albedo (Bonan *et al*., 1992; Thomas & Rowntree, 1992; Chalita & Le Treut, 1994; Douville & Royer, 1996). This suggests that decreased forest cover may have played a role in the onset of the last glaciation (Gallimore & Kutzbach, 1996) and likely reinforced the cold climate of the last glacial maximum 21 000 years ago (Crowley & Baum, 1997). In contrast, the northward mid-Holocene expansion of boreal forest in response to climate warming accentuated the warming (Foley *et al*., 1994).

In contrast to these studies using prescribed vegetation, global vegetation models have been coupled interactively with climate models. One approach known as asynchronous equilibrium coupling uses relationships between climate and biogeography to change vegetation (Henderson-Sellers, 1993). Studies utilizing this type of coupling show the importance of the treeline in initiating the last ice age (de Noblet *et al*., 1996), reinforcing the cold high latitude climate of the last glacial maximum (Kubatzki & Claussen, 1998), and reinforcing the mid-Holocene high latitude warming (Texier *et al*., 1997). Other studies show that the greening of the Sahara enhanced the summer monsoon 6000 years ago (Claussen & Gayler, 1997; Texier *et al*., 1997; de Noblet-Ducoudré *et al*., 2000) and that the choice of the initial vegetation cover of desert or forest can lead to different simulated climate (desert–dry, forest–wet) in the western Sahara (Claussen, 1994, 1997, 1998; Claussen *et al*., 1998; Kubatzki & Claussen, 1998).

Other models known as dynamic global vegetation models (DGVMs) simulate transient vegetation dynamics and are synchronously coupled to climate models (Foley *et al*., 1998). The integrated biosphere simulator (IBIS) (Foley *et al*., 1996; Kucharik *et al*., 2000) epitomizes the coupling of such a model to a climate model. One application of this model simulated the last glacial maximum. The cold, dry glacial climate reduced forest cover in the tropics, which warmed temperature and decreased precipitation, and reduced high latitude forest cover, which further cooled temperature (Levis *et al*., 1999). Another application showed that greater precipitation in North Africa 6000 years ago is sufficient to sustain a northward encroachment of plants into desert and that this enhances precipitation (Doherty *et al*., 2000). Other simulations with a doubling of atmospheric CO_2 from preindustrial levels found large changes in climate as a result of vegetation changes (Levis *et al*., 2000).

These studies show amplification by vegetation through energy, moisture, and momentum fluxes of the climate response to changes in insolation or atmospheric CO_2. Biogeochemical feedbacks are only now being included in climate models. For example, the northward expansion of boreal forest into tundra decreases surface albedo and removes carbon from the atmosphere. The climate cooling resulting from lower atmospheric CO_2 concentration may offset the warming from reduced surface albedo (Betts, 2000). Claussen *et al*. (2001) contrasted the biogeophysical and biogeochemical effects of tropical and boreal deforestation. Tropical deforestation warms climate due to a reduction in evapotranspiration and release of carbon to the atmosphere. Boreal deforestation cools climate as a result of the snow–vegetation albedo feedback, but warms climate from carbon emission. A climate simulation with the global carbon cycle found that dieback of tropical forests as a result of a drier, warmer climate with higher atmospheric CO_2 releases carbon to the atmosphere that accentuates the climate change (Cox *et al*., 2000).

The purpose of this study is to describe and test a vegetation dynamics model that can be used to study vegetation feedback on climate in the Community Climate System Model. The Community Climate System Model is a coupled atmosphere–land–ocean–sea ice model (Blackmon *et al*., 2001). Critical to including interactive vegetation is the linking of vegetation dynamics to the land surface processes in the climate model. The land model used here is the National Center for Atmospheric Research (NCAR) Land Surface Model (LSM) (Bonan 1996, 1998; Bonan *et al*., 2002a). We added vegetation dynamics using concepts from the Lund–Potsdam–Jena (LPJ) DGVM (Cramer *et al*., 2001; McGuire *et al*., 2001; Smith *et al*., 2001; Sitch *et al*., 2003). Our objective is to show that simulated biogeography and vegetation dynamics compare favorably to observed biogeography and generalized patterns of forest succession. We emphasize vegetation composition and structure, which control biogeophysical feedbacks, but also discuss aspects of the carbon cycle.

Methods and model description

The NCAR LSM simulates energy, moisture, and momentum fluxes between the land and atmosphere, the hydrologic cycle, and soil temperature (Bonan, 1996, 1998; Bonan *et al*., 2002a, b). Processes are simulated with a 20 min time step to allow near instantaneous coupling with the atmosphere and to resolve the diurnal cycle. As described by Bonan (1995) and Craig *et al*. (1998), the model provides a consistent treatment of energy exchange, evapotranspiration, and carbon

exchange by plants, a defining characteristic of the latest generation of land models (Sellers *et al*., 1997), by linking photosynthesis (Farquhar *et al*., 1980) with stomatal conductance (Collatz *et al*., 1991, 1992).

The model represents spatial heterogeneity in land cover by dividing each grid cell into four land cover types: glacier, lake, wetland, and vegetation (Bonan *et al*., 2002a, b). The vegetated portion of the grid cell is further divided into several patches of plant functional types. Multiple plant functional types can co-occur in a grid cell so that, for example, a mixed broadleaf deciduous and needleleaf evergreen forest may consist of patches of broadleaf deciduous trees, needleleaf evergreen trees, and other vegetation. Each patch, while sharing the grid cell, is parameterized as a separate column for energy and water calculations. Without vegetation dynamics, plant functional type abundance and leaf area in a grid cell are obtained from satellite data products (Bonan *et al*., 2002a, b).

The LPJ DGVM (Cramer *et al*., 2001; McGuire *et al*., 2001; Sitch *et al*., 2003) also characterizes vegetation as patches of plant functional types that occupy a portion of a grid cell. Hence, the vegetation dynamics of LPJ can be readily incorporated into LSM. LPJ couples fast hydrological and physiological processes with slower ecosystem processes using time-scales of daily (soil water, soil temperature, snow, canopy physiology, phenology), monthly (soil microbial processes), and yearly (vegetation dynamics). In coupling LSM and LPJ, we omitted fast LPJ processes already present in LSM (canopy physiology, snow, and soil physics), altered LPJ algorithms to meet the requirements of a climate model (phenology), and scaled LPJ's daily and monthly respiration to fit LSM's 20 min coupling with the atmosphere. We retained LPJ's daily time step for leaf phenology and LPJ's annual time step for changes in community composition and ecosystem structure.

The resulting model, which we refer to as LSM–DGVM to distinguish it from the original LSM and LPJ models and to highlight the addition of the DGVM, integrates atmospheric and ecological processes across multiple time-scales (Fig. 1). It operates in a similar fashion to LPJ, but with LSM's more complex and diurnally resolved parameterizations. New processes in LSM–DGVM from this integration of models are respiration, allocation, biomass turnover, litterfall, mortality, aboveground competition, fire, establishment, and leaf phenology. Sitch *et al.* (2003) describe these processes, which are summarized as follows.

Plant functional types

As in LPJ, LSM–DGVM divides vegetation into homogeneous, dynamic patches of plant functional types. Each plant functional type is represented by an average individual plant with biomass, crown area, height, and stem diameter (trees only), by the number of individuals in the population, and by the fractional cover of the population in the grid cell. There is no representation of age or size classes. Woody plant functional types (trees) are divided into foliage, sapwood, heartwood, and fine root carbon pools. Herbaceous plant functional types (grasses) have only foliage and fine roots. The leaf area index is calculated from foliage carbon using a specific leaf area and normalized by the crown area.

We use 10 plant functional types, all of which may co-occur in a grid cell depending on the climate. Two tropical trees, three temperate trees, and two boreal trees are differentiated by bioclimatology, leaf form (broadleaf, needleleaf), phenology (evergreen, summergreen, raingreen), physiology, and response to disturbance. Three grasses are distinguished by bioclimatology and photosynthetic pathway (C_3, C_4). The plant functional types are similar to those used in versions of LPJ and are a subset of those used in LSM. Leaf optics, photosynthesis, and morphology are standard LSM parameters (Bonan *et al*., 2002b). Bioclimatic limits for survival and establishment (Table 1) and parameters governing the vegetation dynamics (Table 2) are as in LPJ, except as noted.

Gross primary production

The gross primary production is calculated every 20 min using the LSM photosynthesis–conductance parameterization (Farquhar *et al*., 1980; Collatz *et al*., 1991, 1992; Bonan, 1995; Craig *et al*., 1998) (Fig. 1). This leaf-level parameterization is scaled over the canopy by partitioning the canopy into sunlit and shaded leaves. Values of the maximum rate of carboxylation at 25 °C for each plant functional type (Bonan *et al*., 2002b) are consistent with the canopy scaling and were obtained from published estimates (Wullschleger, 1993; Kucharik *et al*., 2000).

Respiration

The net primary production of the average individual for each plant functional type is the difference between carbon uptake during gross primary production and carbon loss during maintenance and growth respiration. Respiration is calculated every 20 min using LPJ algorithms scaled from LPJ's daily time step to our model's 20 min time step (Fig. 1). A base maintenance respiration rate per unit nitrogen (Table 2) is adjusted for tissue C : N ratio (Table 2) and temperature. The vegetation temperature controls foliage and stem respiration; the soil temperature controls root respiration.

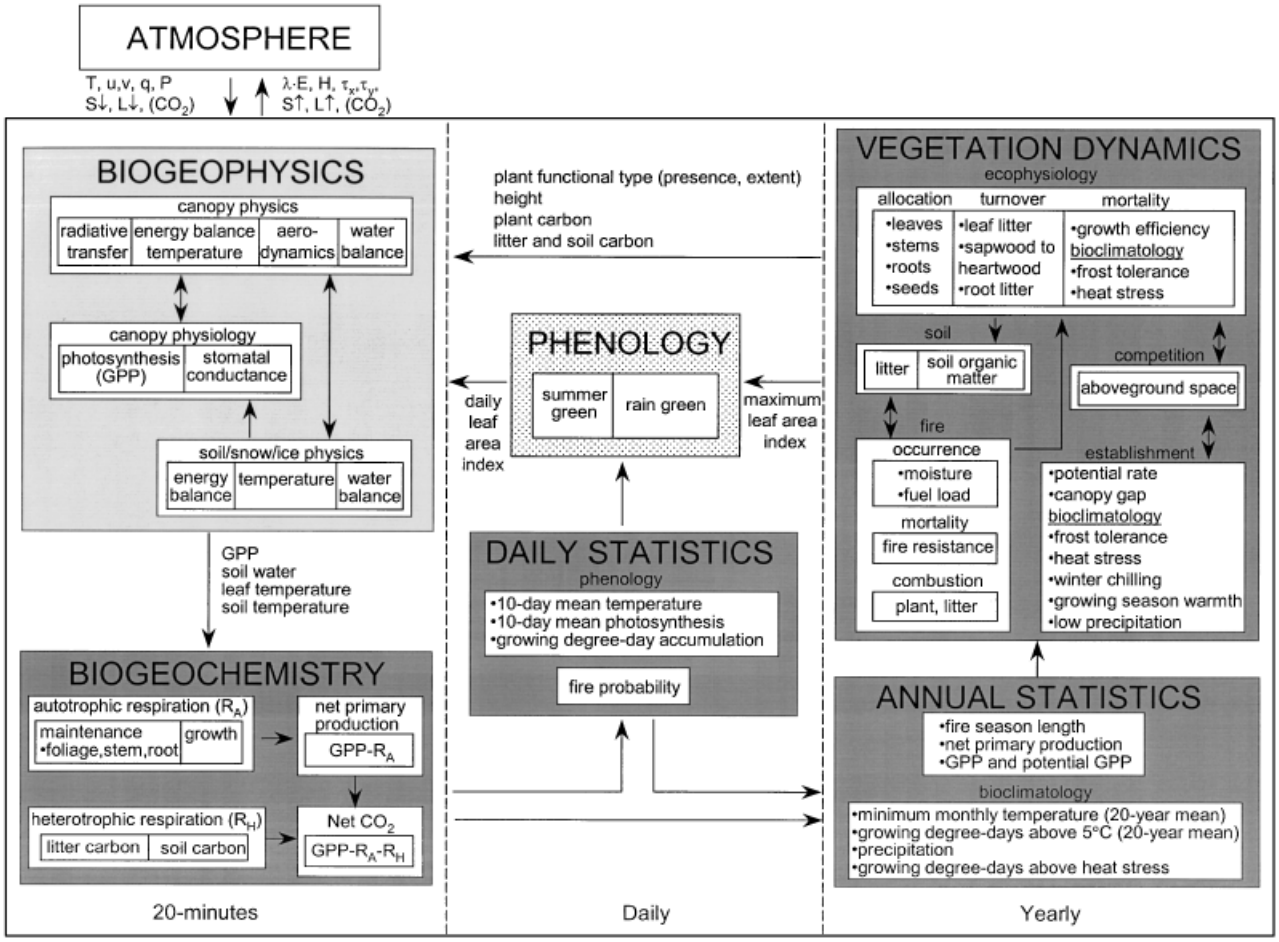

Fig. 1 Components of LSM–DGVM showing the coupling between fast processes such as energy exchange, photosynthesis, and respiration and slower processes such as tissue turnover, mortality, establishment, and disturbance. The biogeophysics (lightly shaded) is the core LSM. To this we added biogeochemistry, vegetation dynamics, and associated daily and annual statistics (all darkly shaded) using concepts from LPJ (Sitch *et al*., 2003). The daily phenology (stippled) is based on Kucharik *et al*. (2000). The model is forced with atmospheric temperature (T), winds (u, v), humidity (q), precipitation (P), and incoming solar ($S\downarrow$) and longwave ($L\downarrow$) radiation. It returns to the atmosphere latent heat (λE), sensible heat (H), surface stresses (τ_x, τ_y), reflected solar radiation ($S\uparrow$), and emitted longwave radiation ($L\uparrow$). When the carbon cycle is included, CO_2 is also exchanged.

Our tropical plants have a higher rate of respiration than in LPJ, while our boreal plants have lower respiration (Sitch *et al*., 2003). This was necessary due to our high maximum rate of carboxylation for tropical trees and low maximum rate of carboxylation for boreal trees (Bonan *et al*., 2002b). After accounting for maintenance respiration, 25% of the remaining carbon is subtracted for growth respiration (Sitch *et al*., 2003).

To complete the carbon cycle, heterotrophic respiration is also simulated by scaling the LPJ parameterization to our 20 min time step (Sitch *et al*., 2003). Above- and belowground litter pools receive litter input annually from the annual vegetation dynamics. Decomposition of these pools is calculated at the 20 min time step and results in two soil organic carbon pools (fast and slow). The rate of decomposition of litter and soil carbon depends on litter quality, soil temperature, and soil moisture. The nitrogen cycle is not included.

Allocation and biomass turnover

The net primary production is summed annually to update plant carbon (Fig. 1; Sitch *et al*., 2003). Ten percent of the annual net primary production is subtracted as a reproductive cost and transferred to aboveground litter to ensure conservation of carbon. The remaining carbon minus turnover loss is added to foliage, sapwood, heartwood, and root mass according to the following allometric rules for the average plant

Table 1 Bioclimatic parameters for survival and establishment

	Survival		Establishment		
Plant functional type	T_c (°C)	T_{hs} (°C)	T_w (°C)	GDD	P_{min} (mm yr^{-1})
Trees					
Tropical broadleaf evergreen tree (BET)	15.5	–	–	–	100
Tropical broadleaf deciduous tree (BDT)	15.5	–	–	–	100
Temperate needleleaf evergreen tree (NET)	−2.0	–	22.0	900	100
Temperate broadleaf evergreen tree (BET)	3.0	–	18.8	1200	100
Temperate broadleaf deciduous tree (BDT)	−17.0	–	15.5	1200	100
Boreal needleleaf evergreen tree (NET)	−32.5	23	−2.0	600	100
Boreal deciduous	–	23	−2.0	350	100
Grasses					
C_4	15.5	–	–	–	100
C_3	−17.0	–	15.5	–	100
C_3 arctic	–	–	−17.0	–	100

Only plant functional types that survive can establish. T_c, coldest minimum monthly air temperature (20-year running mean) for survival of established plants; T_{hs}, heat stress air temperature for survival; T_w, warmest minimum monthly air temperature (20-year running mean) for establishment of new plants; GDD, minimum annual growing degree-days above 5 °C (20-year running mean) for establishment; P_{min}, minimum annual precipitation for establishment.

functional type individual: leaf area is proportional to sapwood area (Table 2); leaf mass is proportional to root mass, with greater allocation to roots as water stress increases (Table 2); and height and crown area are allometric functions of stem diameter. In contrast to LPJ, which calculates a leaf-to-root ratio from the ratio of soil water supply to potential demand, we calculate this from the ratio of actual gross primary production to the potential production assuming unlimited soil water. Simpler allometric rules are used for herbaceous plants. For herbaceous plants, we removed the dependence of leaf-to-root ratio on water stress and instead used a fixed ratio of 0.75 (discussed further in the results).

Biomass turnover is inversely proportional to a turnover period (Table 2). Foliage and root turnover contribute to annual litterfall. Sapwood turnover accumulates as heartwood. Heartwood is transferred to aboveground litter upon mortality or is consumed during fire.

Mortality

Mortality transfers carbon to litter (Fig. 1; Sitch *et al.*, 2003). Herbaceous plants complete their life cycle in 1 year. Among woody plants, mortality reduces the population density. All individuals die if the average individual has a negative biomass increment. Otherwise, mortality is inversely related to growth efficiency, constrained to a maximum mortality rate (Table 2). This is 1% per year (Sitch *et al.*, 2003), except for boreal deciduous trees, which we increased to a maximum mortality of 3% per year to reflect their short longevity (discussed further in the results).

Bioclimatic rules kill established plants (Sitch *et al.*, 2003). To mimic tolerance of cold temperatures, established plants die when a 20-year running mean of the minimum monthly temperature is less than some threshold (Table 1). The 20-year period prevents large year-to-year fluctuation in community composition. In addition, heat stress, defined by the annual degree-days above 23 °C for boreal trees (Table 1), kills some percent of the population.

Aboveground competition

Competition for light also causes mortality and occurs based on the plant functional type's foliage projective cover, which is also the fractional extent of the patch in the grid cell (Sitch *et al.*, 2003). If the foliage projective cover summed over all plant functional types exceeds one, woody plants are favored over herbaceous plants as a result of their dominant position in the canopy. If the summed foliage projective cover of woody plants exceeds 0.95, the density of these individuals is reduced in a self-thinning-like process, favoring plant functional types with a higher annual increment in foliage projective cover.

LSM–DGVM does not represent belowground competition for water among plant functional types because it calculates the soil water balance separately for every subgrid patch. This is in contrast to LPJ, which uses one soil column per model grid cell.

Table 2 Parameters for vegetation dynamics

Plant functional type	Phenology	Specific leaf area ($cm^2\,g\,C^{-1}$)	Leaf-to-sapwood area ($m^2\,cm^{-2}$)	Unstressed leaf-to-root ratio	Turnover (years)			Maximum mortality ($\%\,yr^{-1}$)	Respiration ($g\,C\,g\,N^{-1}\,day^{-1}$)	C:N			Maximum establishment ($individuals\,m^{-2}\,yr^{-1}$)	Fire	
					Leaf	Stem	Root			Leaf	Stem	Root		Fuel moisture	Resistance
Trees															
Tropical BET	E	217	0.8	1.00	2	20	2	1	0.027	29	330	29	0.24	0.3	0.12
Tropical BDT	R	411	0.8	1.00	1	20	1	1	0.027	29	330	29	0.24	0.3	0.50
Temperate NET	E	217	0.8	1.00	2	20	2	1	0.066	29	330	29	0.24	0.3	0.12
Temperate BET	E	299	0.8	1.00	1	20	1	1	0.066	29	330	29	0.24	0.3	0.50
Temperate BDT	S	411	0.8	1.00	1	20	1	1	0.066	29	330	29	0.24	0.3	0.12
Boreal NET	E	217	0.8	1.00	2	20	2	1	0.033	29	330	29	0.24	0.3	0.12
Boreal deciduous	S	411	0.8	1.00	1	20	1	3	0.033	29	330	29	0.24	0.3	0.12
Grasses															
C_4	–	299	–	0.75	1	1	2	1	0.066	29	–	29	–	0.3	–
C_3	–	299	–	0.75	1	1	2	1	0.066	29	–	29	–	0.3	–
C_3 arctic	–	299	–	0.75	1	1	2	1	0.066	29	–	29	–	0.3	–

See Table 1 for a definition of the plant types. Phenology denotes evergreen (E), raingreen (R), or summergreen (S) leaf phenology. Specific leaf area is calculated from leaf longevity (Sitch *et al.*, 2003). Fuel moisture is the fraction of soil water-holding capacity above which fire does not spread. Resistance is the fraction of individuals exposed to fire that survive.

Fire

Fires are simulated annually (Fig. 1). The occurrence and effect of fire depends on fuel load and moisture (Thonicke *et al.*, 2001; Sitch *et al.*, 2003). A minimum fuel load of $200\,g\,C\,m^{-2}$ is required for combustion. The threshold moisture above which fire will not spread can vary among plant functional types, reflecting different fuel flammability, but is currently always 30% of the available water-holding capacity (Table 2). The percent of a plant functional type population killed within the fractional area burnt depends on fire resistance (Table 2). Herbaceous plants complete their life cycle in 1 year, and there is no explicit mortality from fire. Carbon of killed individuals and of consumed aboveground litter is released to the atmosphere.

Establishment

Establishment of new individuals occurs annually after all other processes (Fig. 1; Sitch *et al.*, 2003). For woody plants, a maximum rate of establishment (Table 2) is scaled for the fraction of the grid cell not covered by woody vegetation, thereby limiting establishment to gaps in the canopy. Establishment of herbaceous plants is limited to the nonvegetated portion of the grid cell.

Several bioclimatic rules constrain regeneration (Table 1). Plants must survive in the current climate to regenerate. No establishment occurs in grid cells with annual precipitation less than 100 mm. Regeneration is prohibited when the 20-year running mean of the minimum monthly temperature is greater than an upper threshold, mimicking a winter chilling requirement. Growing season warmth requirements are represented by annual growing degree-days. Establishment is precluded when this is less than a specific limit.

Daily phenology

The leaf area index is updated daily and depends on temperature, soil water, and plant productivity, ranging from zero up to a maximum value set by the annual vegetation dynamics (Fig. 1). Woody plants utilize evergreen, summergreen, or raingreen phenologies (Table 2). Grasses have no assigned phenology. We did not use the phenology of LPJ because LPJ's summergreen phenology requires knowledge of the warmest and coldest months of the year. This information is not available in a climate model until the end of each year. Also, LPJ's raingreen phenology uses concepts of water supply vs. potential demand, which are not in LSM.

Instead, we used phenologies similar to Kucharik *et al.* (2000). Summergreen trees grow leaves when the

accumulated growing degree-days above 0 °C exceed 100. Leaf emergence occur over a period equal to 50 degree-days. Leaf senescence occurs when the 10-day running mean air temperature drops below a threshold. This threshold is the larger of two temperatures: 0 °C or 5 °C warmer than the coldest 10-day running mean temperature in the year. Leaf drop occurs over 15 days. Raingreen trees always maintain a small residual leaf area and grow new leaves when the 10-day running mean net photosynthesis is positive. Negative net photosynthesis initiates leaf drop. Leaf emergence and senescence occur over 15 days. Similar to LPJ, we enforce a minimum 6-month leaf-off period for raingreen plants. Grasses can exhibit a summergreen, raingreen, or evergreen phenology. Grasses take 5 days to drop(grow) their leaves when the 10-day running mean air temperature is below(above) freezing or the 10-day running mean net photosynthesis is negative (positive).

Model simulations

The model was configured for a global 3° by 3° spatial grid with surface data (soils, lakes, wetlands, and glaciers) as with LSM (Bonan *et al.*, 2002a). The model was integrated for 200 years from an initial condition of bare ground, driven with atmospheric data from the period 1979 to 1998 (Bonan *et al.*, 2002a). The 20-year data were repeated 10 times for the length of the simulation, which introduces periodicity in some results.

The simulation is compared with other models, satellite-derived observations, and ecological syntheses. Simulations of LPJ using the same atmospheric data as LSM–DGVM are shown for comparison. We expect differences between the models because they differ in many processes (e.g., soil and snow physics, photosynthesis) and focus only on large differences. Simulated biogeography of plant functional types and their leaf area index are compared with satellite-derived observations that are used as input to LSM without interactive vegetation (Bonan *et al.*, 2002a). We also aggregate the plant functional types into biomes for comparison with Ramankutty & Foley's (1999) potential vegetation. The global net primary production is compared with a synthesis of models (Cramer *et al.*, 1999, 2001). The biome-averaged net primary production is compared with the IBIS DGVM and observations used to test IBIS (Kucharik *et al.*, 2000). Simulated vegetation dynamics is illustrated for five individual grid cells, where the natural vegetation is tundra, boreal forest, temperate deciduous forest, tropical rainforest, and savanna. The simulated dynamics is compared with general patterns of succession for each biome. These comparisons are qualitative and are not meant to be site-specific comparisons. Our goal is to show that the model reasonably replicates biogeography and vegetation dynamics and may, therefore, be used in climate simulations.

Results and discussion

Global vegetation

The global coverage of plant functional types simulated by LSM–DGVM is similar to that of LPJ (Fig. 2). Grasses initially dominate and decline as trees grow. The peak dominance of C_3 and C_4 grasses is similar in both models, but C_3 grasses decline slower in LSM–DGVM. Abundance at 200 years is similar in both models. Tropical trees attain equilibrium rapidly in both models (about 50 years). The equilibrium values of 10–13% broadleaf evergreen and about 5% broadleaf deciduous trees are similar in both models. In both models, temperate forests are dominated by broadleaf deciduous trees (about 8%); broadleaf and needleleaf evergreen trees each cover less than 5% of land. The greatest difference between models is their simulation of boreal forests. Boreal deciduous and needleleaf evergreen trees each cover about 10% of land at equilibrium in LPJ. In LSM–DGVM, deciduous trees initially dominate, followed by needleleaf evergreen trees.

Figure 3 illustrates global biogeography at several years for LSM–DGVM. Grasses initially dominate in the absence of trees and die back with the establishment of forests. The grasslands of North America, South America, Africa, and central Asia are maintained throughout the simulation. Tropical evergreen trees establish within 50 years. Temperate summergreen trees also establish rapidly (by year 100) in eastern US and Europe. Boreal forests establish over a period of 200 years.

The biogeography of trees after 200 years compares favorably with satellite observations (Fig. 4). Broadleaf evergreen trees are more extensive throughout the tropics compared with observations. High crop cover in this region accounts for some of this discrepancy. In Africa, broadleaf evergreen trees compare favorably with observations in the tropical rainforest, but are overestimated in savannas. Needleleaf evergreen trees have highest abundance in northern Canada and Russia as in the observations, although they extend too far north in Canada. Summergreen deciduous trees attain highest dominance in eastern US, Europe, and Southeast Asia. Observations show much less tree cover in these regions than in the simulations, again in part due to high crop cover. Grass cover is lower than observed, as is apparent in the North American Great Plains.

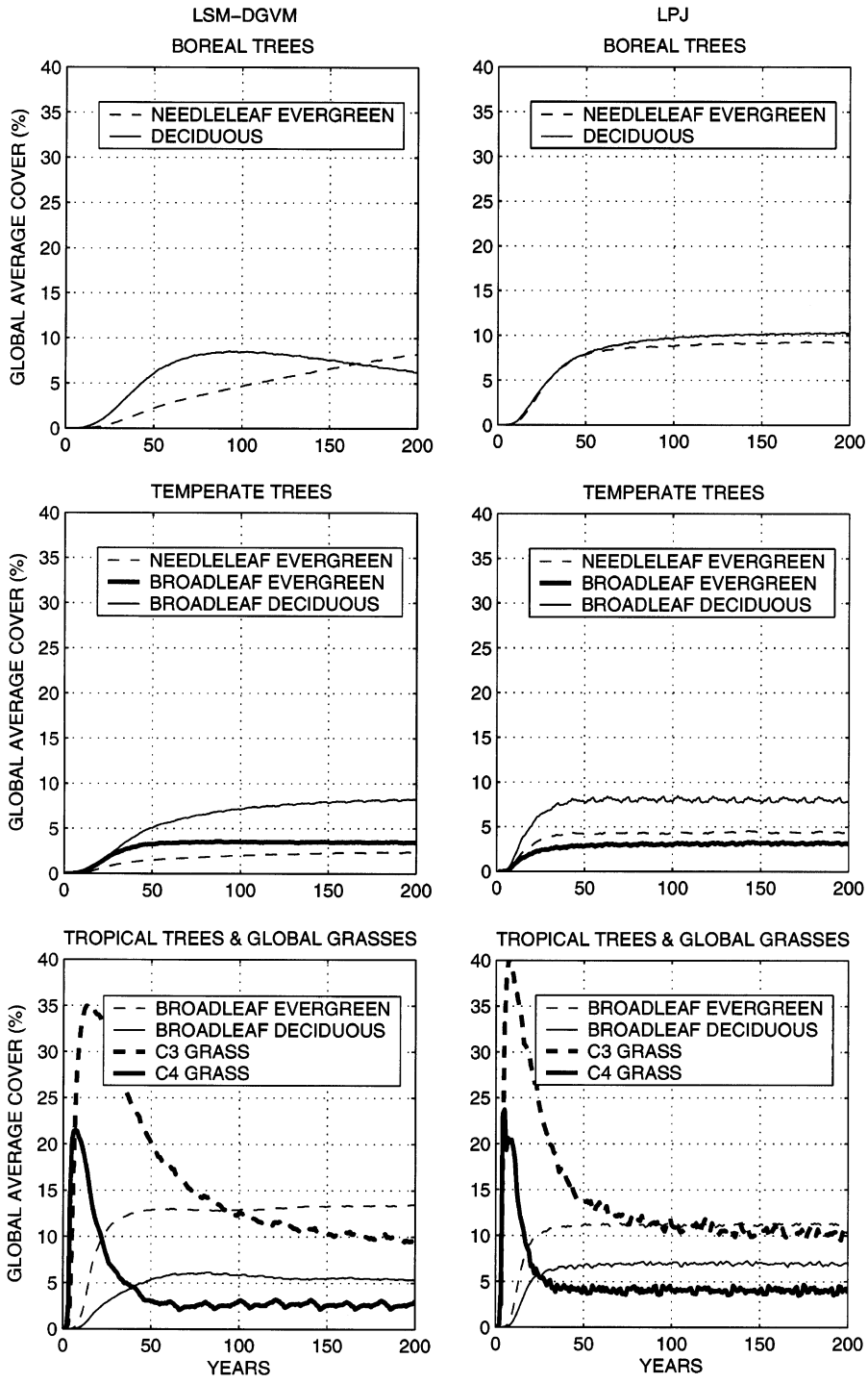

Fig. 2 Global distribution, as a percent of land area including glaciers, of boreal trees (top), temperate trees (middle), tropical trees (bottom), and grasses (bottom) simulated by LSM–DGVM (left) and LPJ (right) over 200 years from initially unvegetated land.

Other DGVMs have higher grass coverage in the Great Plains, southern South America, Africa, and India (Kucharik *et al.*, 2000; Cramer *et al.*, 2001). In general, LSM–DGVM overestimates tree cover at the expense of grasses.

When aggregated to biomes, the simulated biogeography compares well with natural vegetation (Fig. 5, Table 3). One prominent deficiency is a greater extent of tropical forests at the expense of savanna. LSM–DGVM underestimates grass cover due to overestimated tree

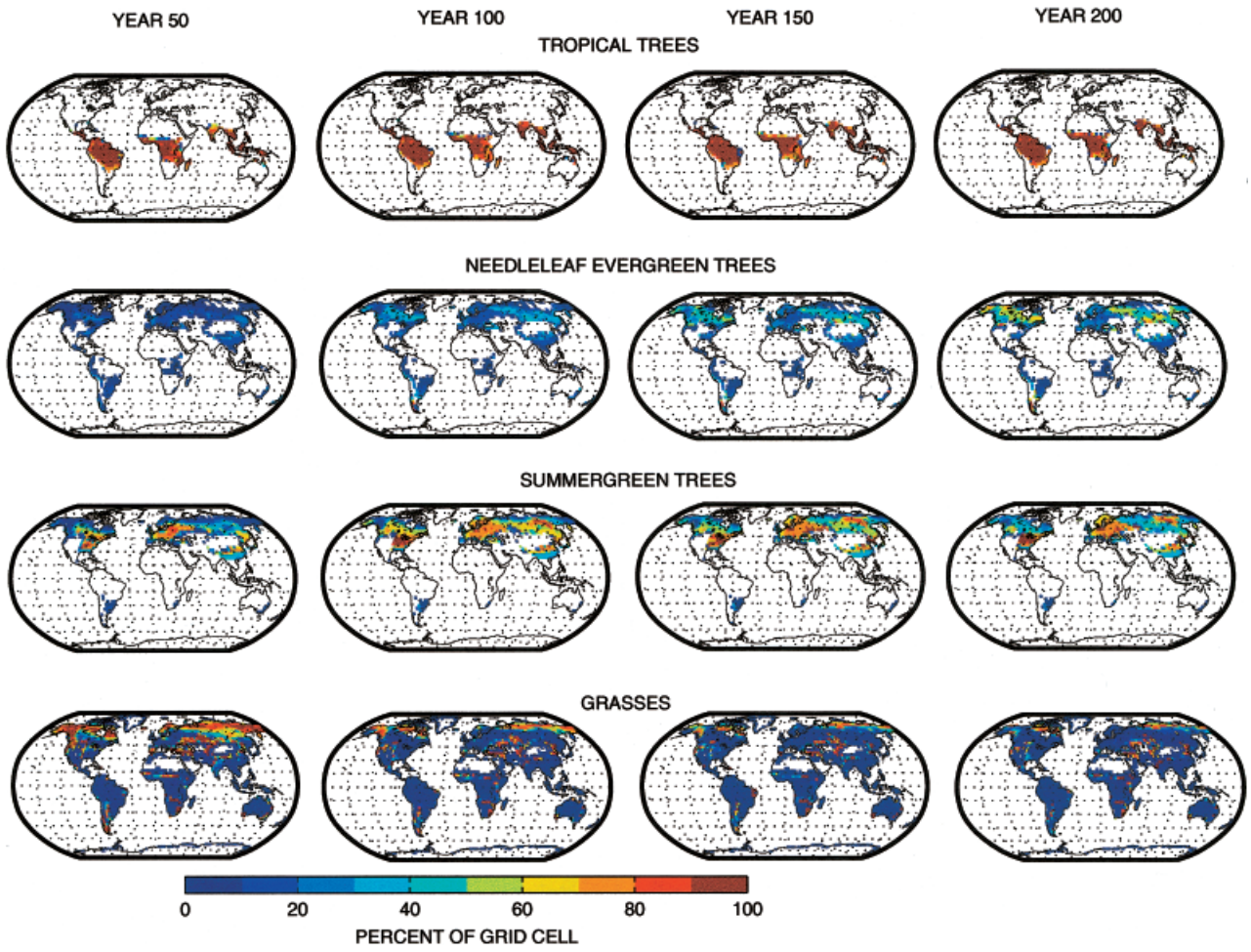

Fig. 3 Geographic distribution of plant functional types, as a percent of grid cell area, simulated by LSM–DGVM at 50 years (left), 100 years (middle left), 150 years (middle right), and 200 years (right).

cover, an issue common with LPJ (Sitch *et al.*, 2003). Areas with a natural vegetation of shrubland are often simulated as desert or grass because LSM–DGVM, and also LPJ, does not simulate shrubs. LSM–DGVM biogeography also compares well with that simulated by six DGVMs (Cramer *et al.*, 2001). Of these models, three have high abundance of grasses in shrubland regions, while two have low grass abundance like LSM–DGVM.

The global net primary production is lower in LSM–DGVM than in LPJ (Fig. 6). The value of 65 Pg C yr^{-1} (averaged over the last 20 years) is comparable to a range of 44–66 Pg C yr^{-1} (mean 54 Pg C yr^{-1}) found in a comparison of 14 net primary production models (Cramer *et al.*, 1999) and 45–60 Pg C yr^{-1} found in a comparison of six DGVMs (Cramer *et al.*, 2001). The net primary production for LPJ is higher than that reported elsewhere (Cramer *et al.*, 2001; McGuire *et al.*, 2001; Sitch *et al.*, 2003) because we used present-day climate and CO_2.

The biome-averaged net primary production compares favorably with simulated values for the IBIS DGVM and with observations (Table 3). The one prominent deficiency is the low productivity of grasslands, which is common also to IBIS. This low productivity in combination with sparse grasslands led us to remove the soil water dependence of herbaceous leaf-to-root ratio (Table 2). However, improving the biogeography of global grasslands hinges more upon reducing tree cover than on increasing herbaceous productivity.

Plant carbon has not attained equilibrium after 200 years in either model (Fig. 6). Leaf and root carbon reach equilibrium quickly. Stem sapwood reaches equilibrium after about 160 years. Heartwood is still accumulating after 200 years in both models.

The evergreen, raingreen, and summergreen phenologies are evident in simulated monthly leaf area index (Fig. 7). Tropical forests along the equator have a high leaf area index throughout the year. Dry forests to the north and south have the highest leaf area during the

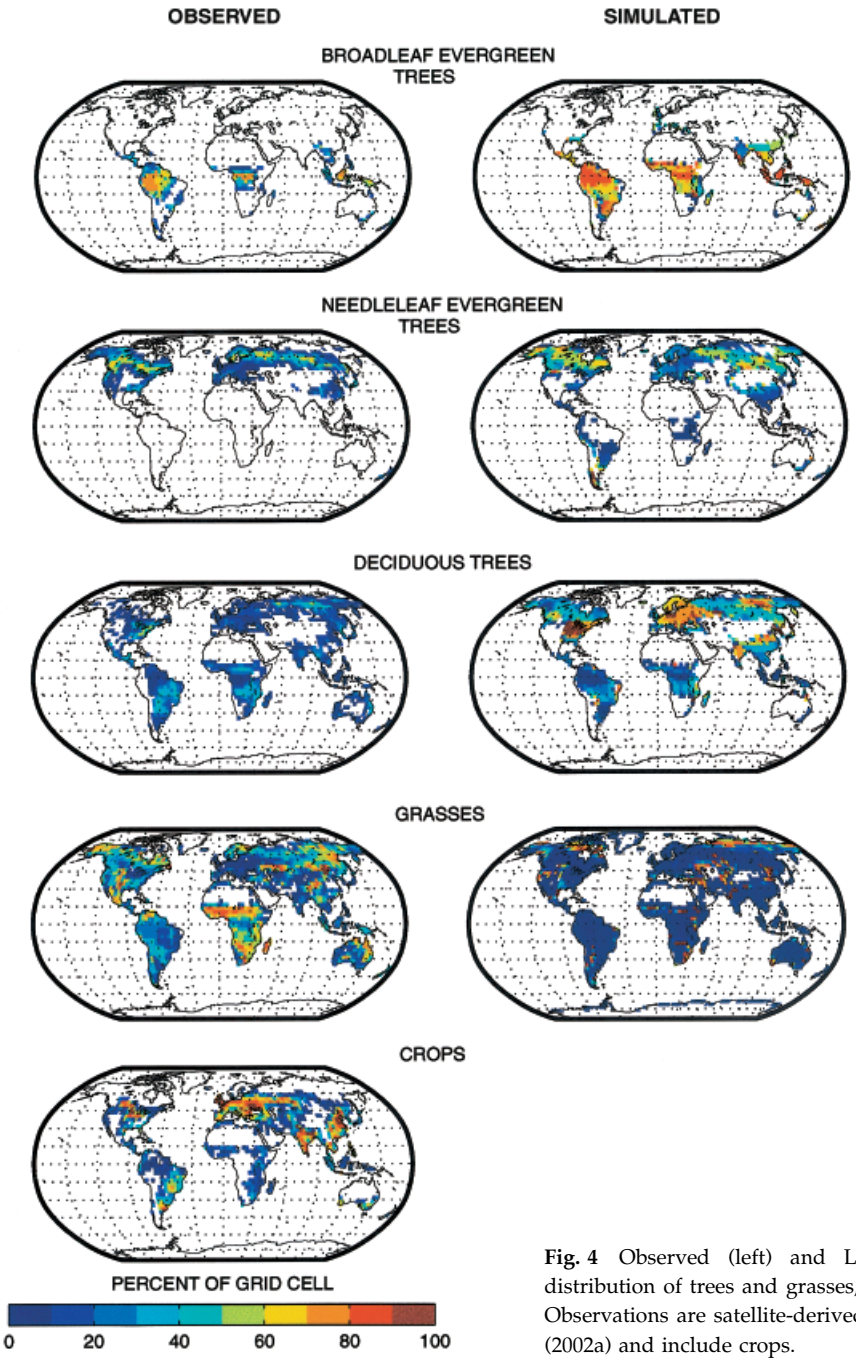

Fig. 4 Observed (left) and LSM–DGVM simulated (right) geographic distribution of trees and grasses, as a percent of grid cell area, at 200 years. Observations are satellite-derived estimates of plant cover from Bonan *et al.* (2002a) and include crops.

rainy season. Temperate, boreal, and arctic regions have summergreen phenology. The summer leaf area index of 3–8 $m^2 m^{-2}$ throughout much of North America, Europe, and Russia is consistent with satellite-derived leaf area (Fig. 8). Forested leaf area index compares favorably with observations of 2–6 $m^2 m^{-2}$ in boreal forests and 1–8 $m^2 m^{-2}$ in temperate forests (Kucharik *et al.*, 2000). However, the simulated leaf area index of 9–10 $m^2 m^{-2}$ throughout the tropics is greater than satellite observations (Fig. 8) and values of 5–8 $m^2 m^{-2}$ reported for tropical forests (Kucharik *et al.*, 2000).

Vegetation dynamics

The dynamics of tundra is limited in that the model represents tundra as herbaceous plants without shrubs or mosses. Thus, the model cannot represent succession in shrub tundra along riverbanks (Bliss & Cantlon,

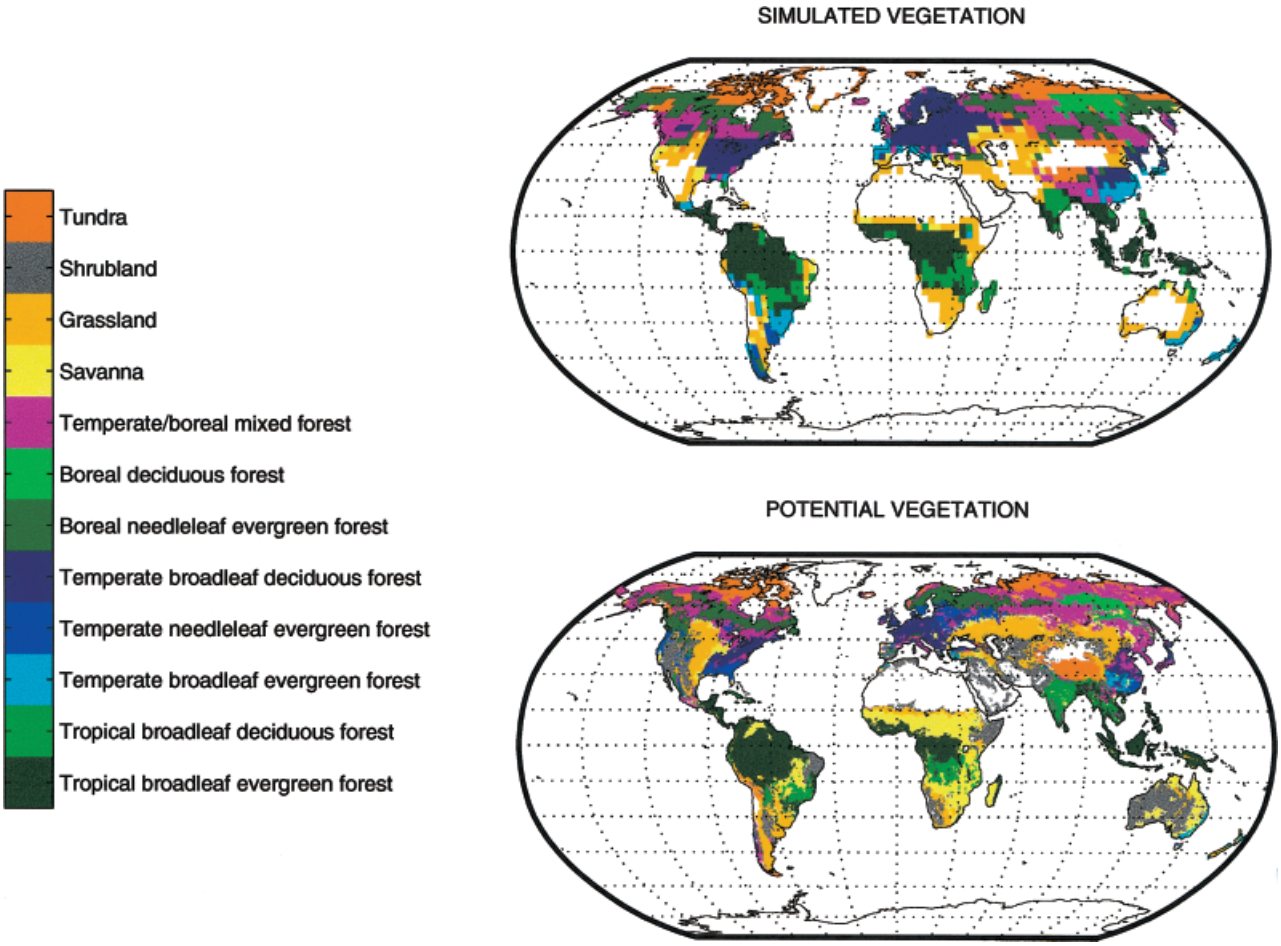

Fig. 5 LSM–DGVM simulated biogeography (top) compared with Ramankutty & Foley's (1999) potential vegetation (bottom). Vegetation type is defined by mixtures of plant functional types in LSM–DGVM and therefore does not necessarily correspond directly to the observed vegetation.

Table 3 Simulated biogeography and net primary production (NPP) for LSM–DGVM compared with observations and that simulated by the IBIS dynamic global vegetation model (Kucharik *et al.*, 2000)

	LSM–DGVM		IBIS		Observations	
Vegetation type	Area (10^6 km^2)	NPP (g C m^{-2} yr^{-1})	Area (10^6 km^2)	NPP (g C m^{-2} yr^{-1})	Area (10^6 km^2)	NPP (g C m^{-2} yr^{-1})
Tropical broadleaf evergreen forest	21.0	1278	19.3	900	16.8	1250 ± 900
Tropical broadleaf deciduous forest	9.4	886	7.7	570	5.8	825 ± 475
Temperate needleleaf evergreen forest	1.3	459	3.3	570	4.8	775 ± 500
Temperate broadleaf evergreen forest	6.0	821	7.2	830	1.1	900 ± 550
Temperate broadleaf deciduous forest	12.6	561	9.7	620	3.6	600 ± 325
Boreal needleleaf evergreen forest	10.6	352	14.5	370	6.0	325 ± 200
Boreal deciduous forest	2.4	362	6.8	330	2.2	425 ± 200
Temperate/boreal mixed forest	11.4	483	4.2	480	14.9	525 ± 275
Savanna	4.7	544	5.3	350	19.1	–
Grassland	18.1	175	21.2	240	14.2	575 ± 475
Tundra	9.3	159	6.2	210	7.0	150 ± 200

Vegetation type is defined by mixtures of plant functional types in LSM–DGVM and therefore does not necessarily correspond directly to the IBIS or observed vegetation. NPP observations are mean ± standard deviation (Kucharik *et al.*, 2000). Observed biogeography is from Ramankutty & Foley (1999).

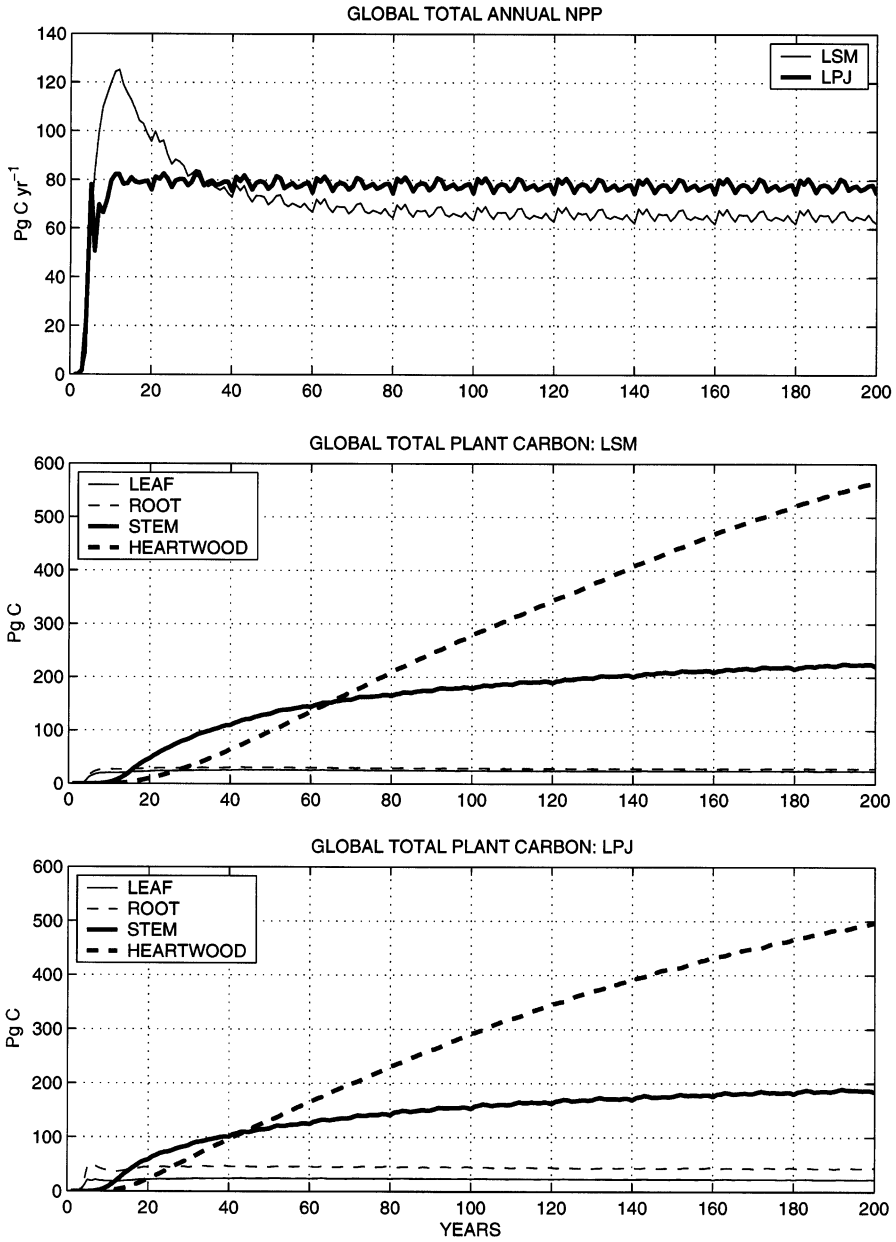

Fig. 6 Global annual carbon fluxes and pools simulated by LSM–DGVM and LPJ over 200 years. Top: net primary production. Middle: leaf, root, stem, and heartwood carbon simulated by LSM–DGVM. Bottom: leaf, root, stem, and heartwood carbon simulated by LPJ. 1 Pg is 10^{15} g.

1957; Bliss, 2000). Elsewhere, however, plant succession in the Arctic is generally not characterized by species replacement (Bliss, 2000). In the low Arctic, vegetation recovery following disturbance occurs over 25 years or less (Bliss, 2000). Tussock tundra recovers to predisturbance levels within 2 years (Wein & Bliss, 1973), 5–6 years (Racine *et al.*, 1987), 5–10 years (Chapin & Chapin, 1980), and 13 years (Fetcher *et al.*, 1984). The recovery of vascular plants occurs over 50–100 years in the high Arctic (Bliss, 2000).

The model captures this recovery of vegetation (Fig. 9). Within less than 25 years, plant cover reaches an equilibrium value of about 80%. The net primary production and plant mass recover more slowly, attaining predisturbance levels after about 40 years. At equilibrium, aboveground plant mass (Table 4) is comparable to observed values of 42–210 g C m^{-2} for wet sedge and tussock tundra (Bliss, 2000, assuming a carbon content of 50% in dry biomass). The simulated root : shoot ratio (1.3 : 1) is less than the observed values

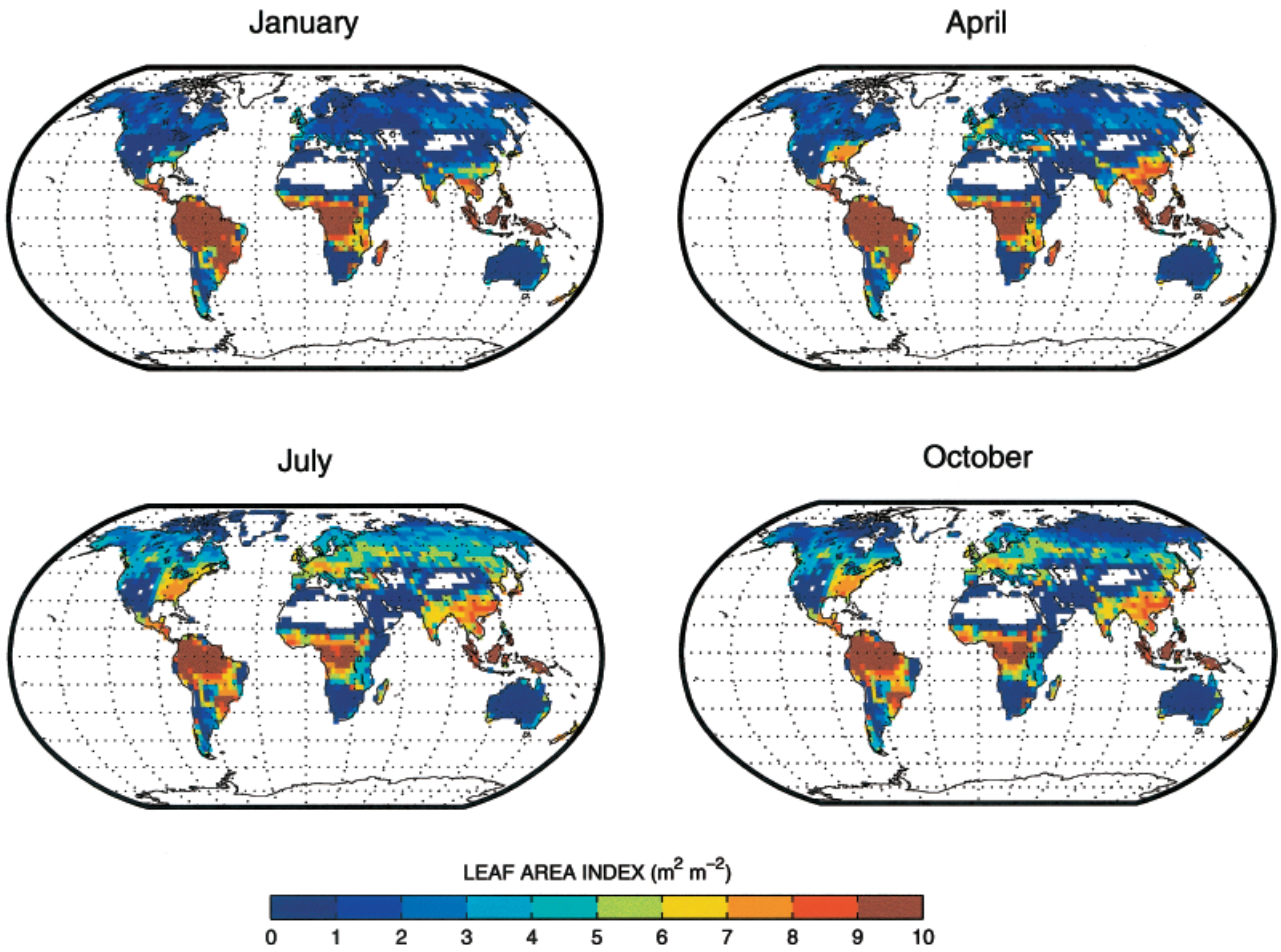

Fig. 7 Monthly leaf area index simulated by LSM–DGVM at 200 years.

of 2 : 1 or 3 : 1 (Bliss, 2000). The simulated tundra is more productive than the reported values of 75–100 g C m^{-2} yr^{-1} (Bliss, 2000).

In the boreal forest of Alaska and Canada, forest communities are a successional mosaic of quaking aspen (*Populus tremuloides* Michx.), paper birch (*Betula papyrifera* Marsh.), white spruce (*Picea glauca* (Moench) Voss), and black spruce (*Picea mariana* (Mill.) B.S.P.), which reflects recovery from disturbance (Van Cleve *et al.*, 1983a, b, 1986, 1991; Bonan, 1989, 1990a, b; Bonan & Van Cleve, 1992). Postfire recovery on warm, upland sites in interior Alaska illustrates the shifting dominance from broadleaf deciduous trees (aspen, birch) to needleleaf evergreen trees (white spruce). Shrubs and tree saplings dominate for about 25 years following fire, when the saplings grow into a dense stand of deciduous trees. These deciduous trees dominate for the next 50 years, although white spruce seedlings and saplings grow in the understory. After about 100 years, the short-lived, fast-growing deciduous trees begin to die and white spruce grows into the canopy.

The model reproduces this succession (Fig. 10). Grasses initially dominate, followed by a rapid decline in grasses and increase in deciduous trees. Deciduous trees attain the greatest cover at 82 years. Thereafter, they decline in cover. The conversion from primarily deciduous to evergreen forest occurs at 145 years, after which evergreen trees increase to 76% cover and deciduous trees decline to 15%. Grasses maintain 9% coverage.

This succession differs from that of LPJ (Fig. 11). LPJ has similar initial dominance by grasses, but needleleaf evergreen trees always dominate over deciduous trees. This is related to the higher net primary production of needleleaf evergreen trees compared to deciduous trees in LPJ (Fig. 11). LSM–DGVM has a lower net primary production for needleleaf evergreen trees than for deciduous trees. With LSM–DGVM, dominance by needleleaf evergreen trees is achieved using a maximum mortality rate for boreal deciduous trees of 3% per year vs. 1% per year for needleleaf evergreen trees. This reflects the short life-span of deciduous trees, but

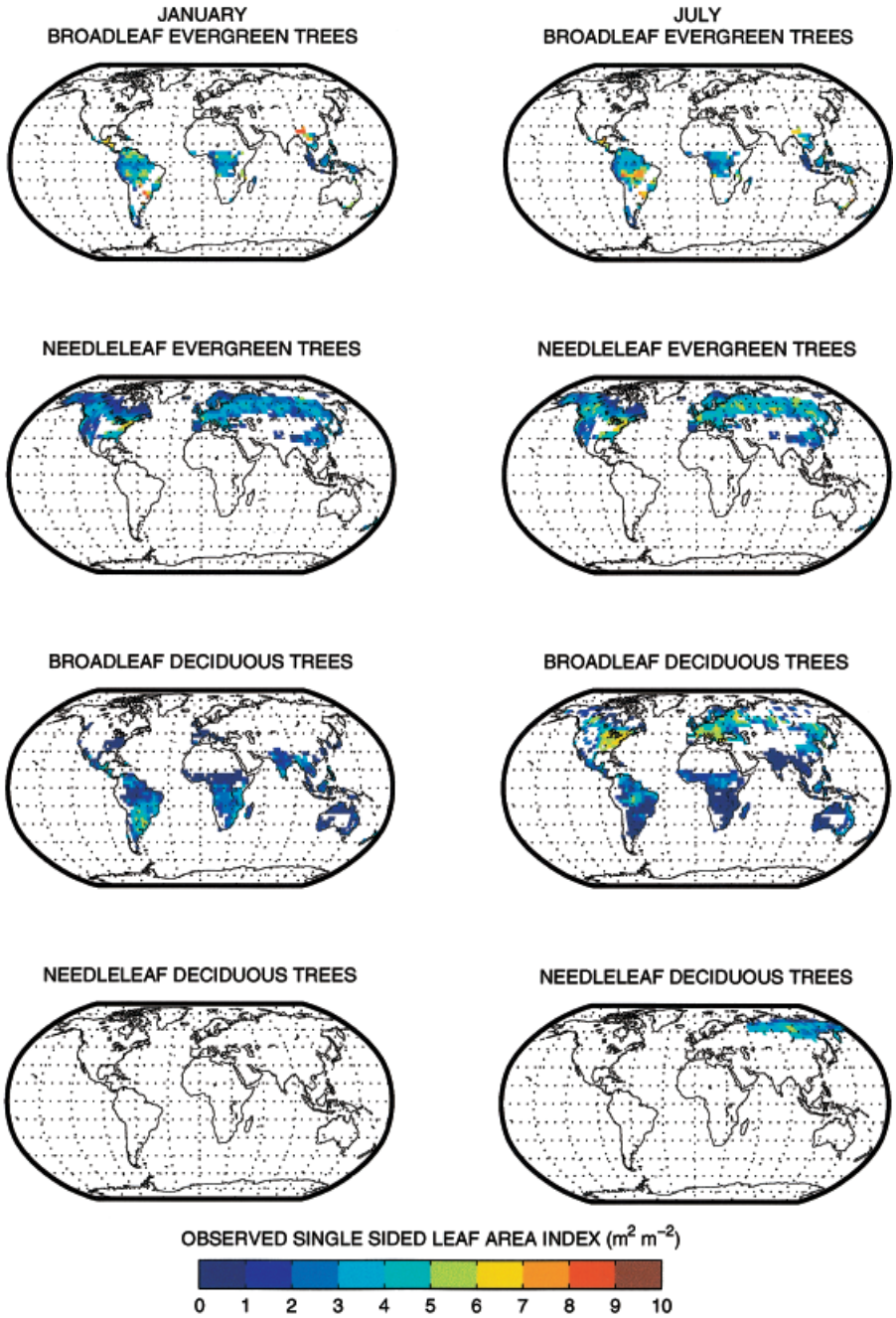

Fig. 8 Satellite-derived leaf area index for January (left) and July (right) for broadleaf evergreen, needleleaf evergreen, broadleaf deciduous, and needleleaf deciduous trees (Bonan *et al.*, 2002a).

is in contrast to LPJ, where a constant 1% per year is used for all plant functional types.

Equilibrium is slowly attained in the boreal forest (Fig. 10). The net primary production reaches constant values by 250–300 years. Foliage and root mass attain equilibrium by about 100 years. Stem sapwood and leaf area attain near constant values by about 500 years. The composition of the forest at 250 years (66% evergreen, 28% deciduous, 5% grass) is close to equilibrium, although this is not attained until about 800 years. The largest trend is in heartwood mass, which accumulates carbon throughout the simulation.

In nature, recurring fires preclude stands much older than 250 years in this region. For this reason, we compare the observed variables to simulated ones at around 250 model years. The simulated net primary

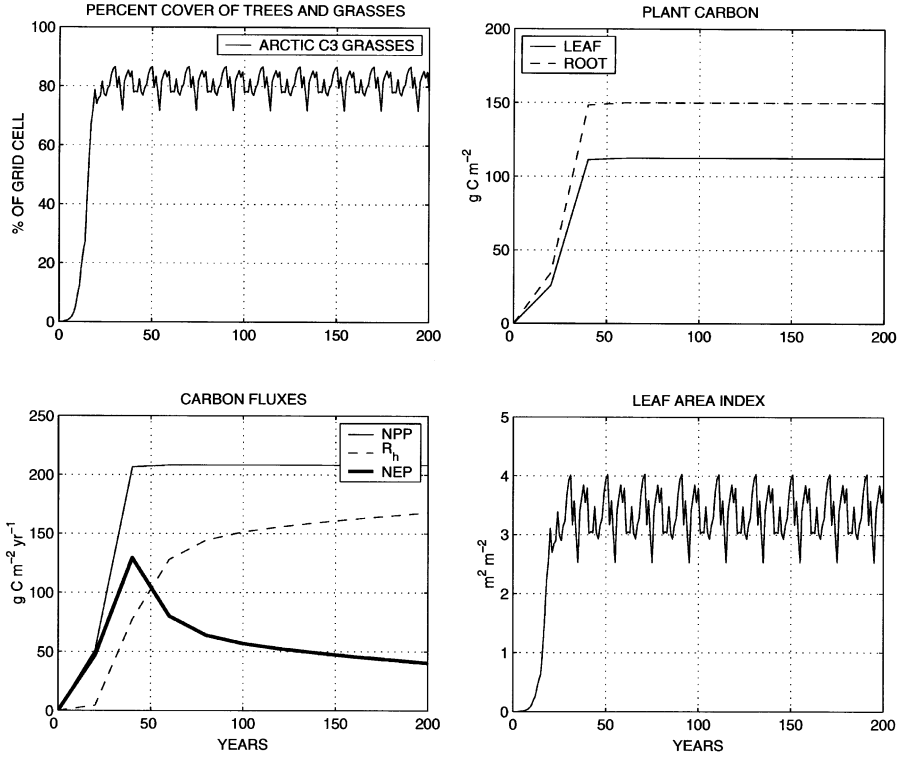

Fig. 9 LSM–DGVM vegetation dynamics from initially bare ground for a grid cell in the Canadian Arctic (65.5°N, 105.5°W). Percent cover is the annual extent of plant functional types in the grid cell. Carbon fluxes and biomass are 20-year averages. Carbon fluxes are shown for net primary production (NPP), heterotrophic respiration (R_H), and net ecosystem production (NEP = NPP – R_H). The leaf area index is the maximum attained each year.

Table 4 Biomass, leaf area index, net primary production (NPP), heterotrophic respiration (R_H), and net ecosystem production (NEP = NPP – R_H) simulated by LSM–DGVM for tundra, boreal forest, northern hardwood forest, and tropical rainforest ecosystems

	Tundra	Boreal forest	Northern hardwood forest	Tropical rainforest
Biomass ($g C m^{-2}$)				
Foliage	112	182	152	667
Sapwood	0	1445	3084	8619
Heartwood	0	8596	15478	21124
Root	150	209	157	674
Leaf area index ($m^2 m^{-2}$)	3.4	3.3	5.9	14.7
NPP ($g C m^{-2} yr^{-1}$)	208	368	603	1672
R_H ($g C m^{-2} yr^{-1}$)	168	356	585	1618
NEP ($g C m^{-2} yr^{-1}$)	40	12	18	54

Data are averaged over the last 20 years of simulations for individual grid cells shown in Figs 9, 10, 12, and 14.

production at this time ($386 g C m^{-2} yr^{-1}$) is similar to observations. Van Cleve *et al*. (1983b) found that aboveground net primary production for white spruce stands near Fairbanks, Alaska, ranges from 119 to $270 g C m^{-2} yr^{-1}$ (assuming a carbon content of 50% in dry biomass) with a mean of $183 g C m^{-2} yr^{-1}$. Ruess *et al*. (1996) subsequently reported a similar mean for floodplain and upland white spruce (183 and $227 g C m^{-2} yr^{-1}$, respectively) and found that fine root production is 49% of total tree production. This gives average estimates of total net primary production of $359 g C m^{-2} yr^{-1}$ for the Van Cleve *et al*. (1983b) study and 359 and $445 g C m^{-2} yr^{-1}$ for the Ruess *et al*. (1996) study. In northern Canada, Gower *et al*. (1997) and Steele *et al*. (1997) estimated total net primary production of two needleleaf evergreen forests to be 222

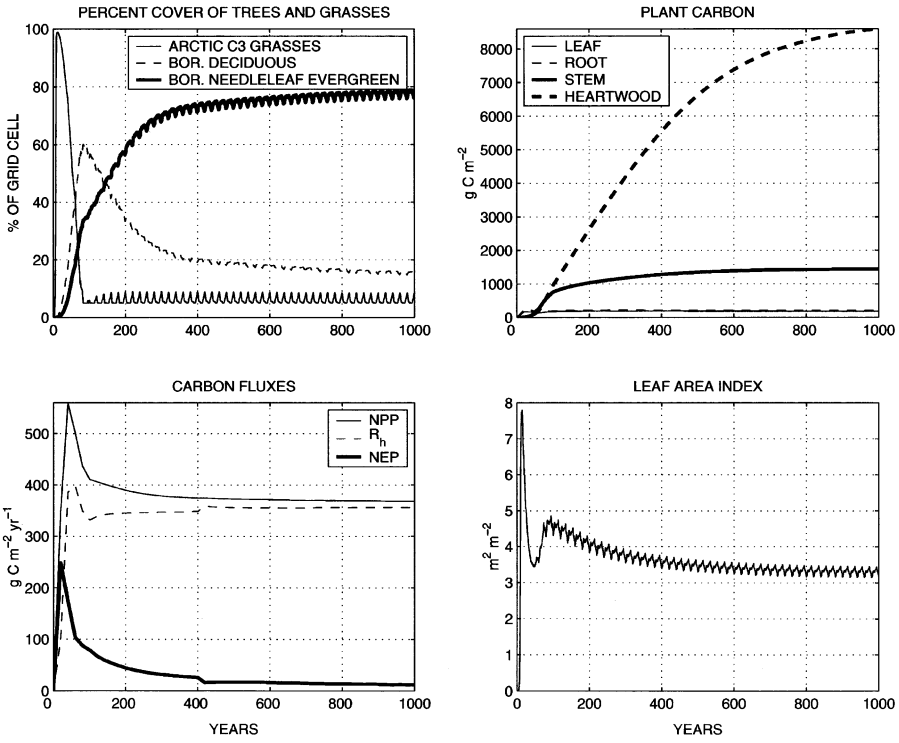

Fig. 10 As in Fig. 9, but for a grid cell in the Canadian boreal forest (60.5°N, 105.5°W).

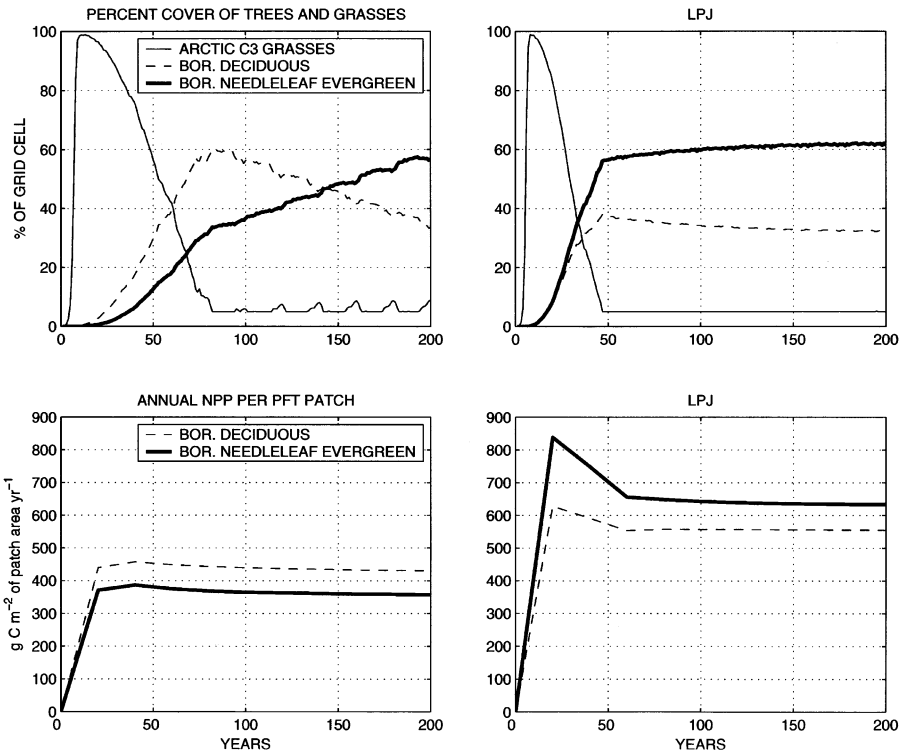

Fig. 11 Boreal forest dynamics simulated by LSM–DGVM (left) and LPJ (right). The top panels show percent cover of plant functional types in the grid cell. The bottom panels show the annual net primary production of tree plant functional types per unit patch area.

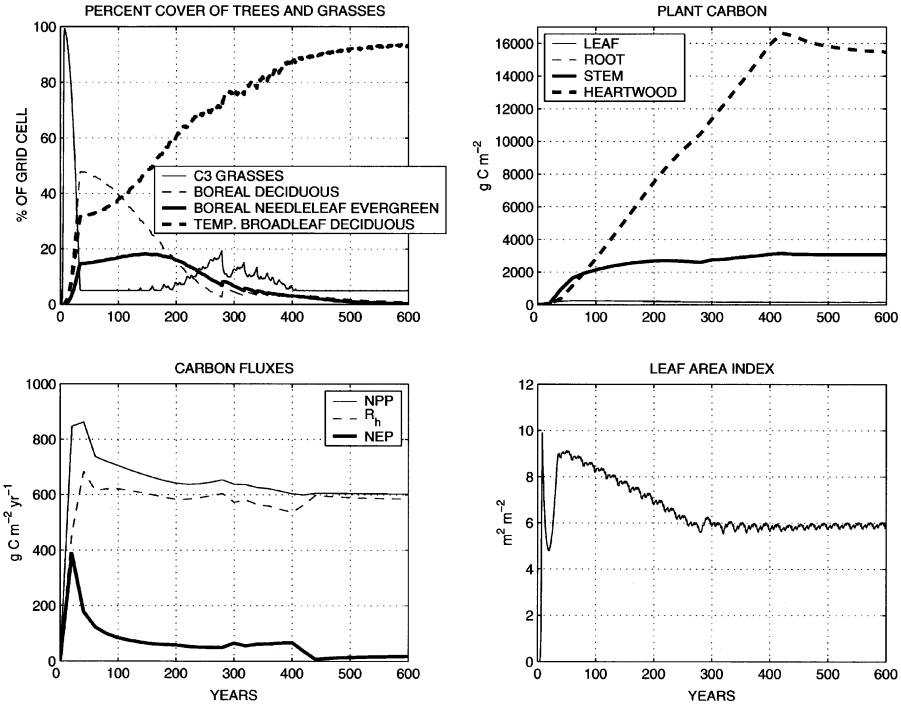

Fig. 12 As in Fig. 9, but for a grid cell in the northern hardwood forest of Northeast US (42.0°N, 74.0°W).

and 286 g C m^{-2} yr^{-1}. Simulated foliage mass (195 g C m^{-2}) is on the low end of average values of 280–624 g C m^{-2} reported for spruce stands in interior Alaska (Van Cleve *et al*., 1983b) and 103–505 g C m^{-2} reported for needleleaf evergreen stands in northern Canada (Gower *et al*., 1997). Sapwood and heartwood mass (4757 g C m^{-2}) is comparable to a range of 2216–7776 g C m^{-2} in interior Alaska and 3556–4924 g C m^{-2} living and standing dead wood in northern Canada (Gower *et al*., 1997). Fine root mass (223 g C m^{-2}) is higher than values of 110–152 g C m^{-2} in interior Alaska (Ruess *et al*., 1996).

The Hubbard Brook study provides a detailed description of succession in northern hardwood forests of New England (Likens *et al*., 1977; Bormann and Likens, 1979). Marks (1974) summarized general changes in community composition following disturbance. During the first 2–3 years following clear-cutting, raspberry and blackberry (*Rubus* species) flourish, complete their life cycle, and decline. These are replaced by pin cherry (*Prunus pensylvanica* L.f.), a common early successional tree. These trees grow fast and are short-lived. Canopy closure occurs rapidly when large seed stores form dense stands. Pin cherry dominates the canopy for the next several years. After about 25–35 years, sugar maple (*Acer saccharum* Marsh.) and American beech (*Fagus grandifolia* Ehrh.), which are tolerant of shade and are able to survive beneath the dense pin cherry canopy, become dominant. Where pin cherry is less dense, it may be co-dominant with other fast-growing species such as yellow birch (*Betula alleghaniensis* Britton) and quaking aspen. Birch and aspen live longer than pin cherry, establish within the first few years following disturbance, and dominate the canopy for several decades before slower growing maple and beech trees reach canopy status. A similar succession is reported by Delcourt & Delcourt (2000), who describe mesic northern hardwood forests as dominated by quaking aspen, paper birch, and balsam poplar (*Populus balsamifera* L.) in the early stages of succession and by sugar maple, American beech, and yellow birch in the late stages of succession.

LSM–DGVM replicates northern hardwood succession (Fig. 12). Grasses initially dominate, followed by boreal deciduous trees. These trees decline in cover and temperate broadleaf deciduous trees dominate by 100 years. Boreal needleleaf evergreen trees maintain relatively low coverage, peaking at 20% early in the simulation and then declining. This is consistent with the observed community composition of Hubbard Brook, where sugar maple, American beech, and yellow birch are the principal tree species, with a small component of other temperate and boreal species (Bormann *et al*., 1970). This succession is quite different from that simulated by LPJ, which gives a primarily deciduous forest with equal amounts of boreal and temperate plant functional types and a high abundance of boreal needleleaf evergreen trees (Fig. 13). The low

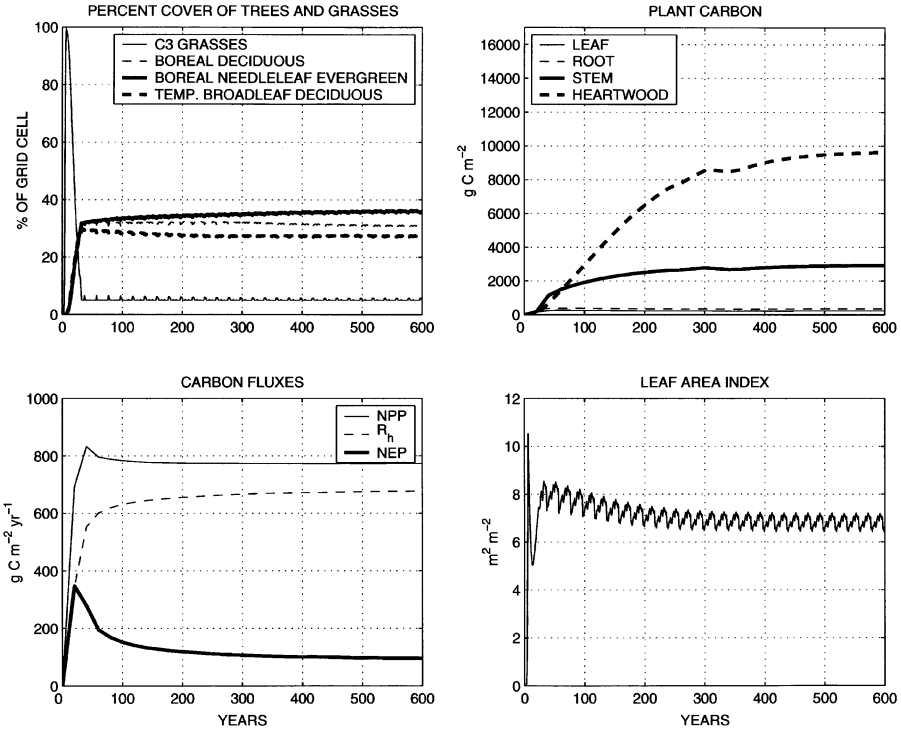

Fig. 13 As in Fig. 12, but for LPJ.

abundance of boreal needleleaf evergreen trees in LSM–DGVM is due to low productivity arising from their low rate of photosynthesis. Boreal deciduous trees decline in abundance over time because of their high mortality (Table 2). The mortality of temperate broadleaf deciduous trees is lower because this plant functional type represents a mix of species from short-lived trees to long-lived maple and beech.

The equilibrium community composition, net primary production, and biomass are attained over a period of 400–600 years (Fig. 12, Table 4). The total net primary production (603 g C m^{-2} yr^{-1}) is comparable to 522 g C m^{-2} yr^{-1} reported by Whittaker *et al.* (1974). The total tree mass (18.9 kg C m^{-2}) is comparable to estimates of 16.2–19.5 kg C m^{-2} (Bormann & Likens, 1979) and 21 kg C m^{-2} for old-growth stands. The leaf area index ($\sim$6 m^2 m^{-2}) is comparable to the range of 5–7 m^2 m^{-2} observed in older forests (Aber, 1979).

LSM–DGVM simulates a tropical broadleaf evergreen forest for a grid cell located in the Amazon (Fig. 14). Grasses attain peak dominance after 5 years. Tropical broadleaf evergreen trees gain dominance rapidly, achieving 81% coverage by 17 years. LPJ has similar vegetation dynamics (not shown), but maintains a lower coverage of broadleaf evergreen trees (65% of grid cell) and higher broadleaf deciduous trees (30%). The simulated forest growth is similar to that observed in tropical rainforests. Richards (1979), Ewel (1983), and Whitmore (1990) describe a succession in which weedy herbaceous plants attain rapid coverage following large-scale disturbance. This initial herbaceous stage does not last long, and pioneer trees establish early. These trees form a closed canopy within a few years, but are short-lived and are replaced by slower-growing, longer-lived species capable of reproducing in shade after about 20 years or so. The succession from pioneer to climax species is not replicated in LSM–DGVM because we allow only one tropical broadleaf evergreen plant functional type.

The net primary production (Table 4) is within the range of observations for tropical broadleaf evergreen forests (mean $\pm$ SD 1250 $\pm$ 900 C m^{-2} yr^{-1}, Kucharik *et al.*, 2000). The leaf area index (Table 4) is greater than values of 5–8 m^2 m^{-2} reported for tropical forests (Kucharik *et al.*, 2000). High leaf area is common throughout tropical forests (Fig. 7). The total plant mass is 31 084 g C m^{-2}, of which two-thirds is heartwood (Table 4). The reliability of tropical forest biomass estimates is poor, but it is likely that the simulated value is high. Schlesinger (1997) reports a mean plant mass of 15 000 g C m^{-2} for tropical wet forests. Brunig (1983) reports average biomass ranges from 15 000 to 32 500 g C m^{-2} (assuming 50% carbon in dry biomass) in tropical rainforests. He cites a value of 19 550 g C m^{-2} in the Amazon, which is thought to be typical of forests in tropical America. Golley (1983) lists

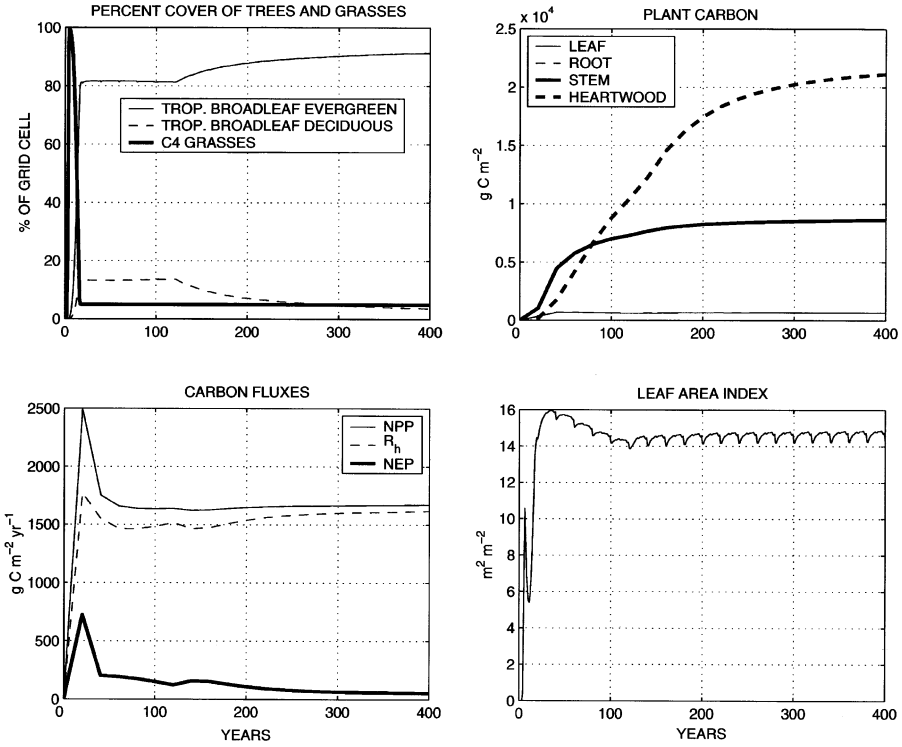

Fig. 14 As in Fig. 9, but for a grid cell in the Amazon (5.0°S, 60.0°W).

values of 18 800 and 21 000 g C m^{-2} (assuming 50% carbon in dry biomass) for two tropical forests in Panama and Brazil. LPJ simulates plant mass of about 19 000 g C m^{-2}, with substantially less sapwood (6000 g C m^{-2}) and heartwood (12 000 g C m^{-2}) than LSM–DGVM. This reflects a lower net primary production (about 1300–1400 g C m^{-2} yr^{-1}), likely due to the greater abundance of deciduous trees.

LSM–DGVM simulates a mixture of tropical broadleaf deciduous trees and C_4 grasses for the savanna grid cell in the African Sahel (Fig. 15). Grasses initially dominate, covering close to 100% of the grid cell after 10–30 years. Thereafter, they decline in coverage and trees increase. By about 80 years, trees are more extensive than grasses. Trees continue to increase in coverage, reaching maximum extent between years 120 and 160. At year 164, trees decline in coverage, ranging from about 60% to 70% of the grid cell for the rest of the simulation, and grasses increase to about 30–40%. The leaf area index is high while grasses dominate, declines and then increases again as trees grow (Fig. 15). After year 164, leaf area index varies regularly from year to year with peak values of about 5 m^2 m^{-2}.

The abrupt change in plant functional type coverage at year 164 is triggered by a large fire that burns 18% of the grid cell (Fig. 15). Prior to this, fires occur sporadically and vary in extent. After year 164, fires are much more frequent and regular. This change in fire behavior is related to changes in soil water. For the first 80 years, when grasses dominate the grid cell, the top 30 cm of soil is depleted of water each year (see annual minimum soil water, Fig. 15). Fires occur each year, but large fires that burn more than 5% of the grid cell only occur in dry years. As trees begin to dominate, leaf area index increases. The maximum soil water content decreases somewhat, but more significantly the soil is not as depleted of water during the year. As the trees mature, they apparently overshoot the leaf area that the site can support. Interannual variability in the prescribed 20-year precipitation cycle has relatively little effect on maximum soil water until years 156–166. As annual precipitation during this 11-year period decreases from a high of 887 mm to a low of 472 mm, maximum soil water decreases leading to the large fire in year 164. Thereafter, a lower leaf area index and a more equal distribution of trees and grasses is maintained.

The savanna simulations demonstrate the importance of fire in maintaining a high abundance of grasses. This is consistent with the ecology of savannas (Walker, 1981; Scholes & Walker, 1993; Sims & Risser, 2000). Additionally, the availability of soil water maintains the balance between grasses and trees (Walker, 1981). In

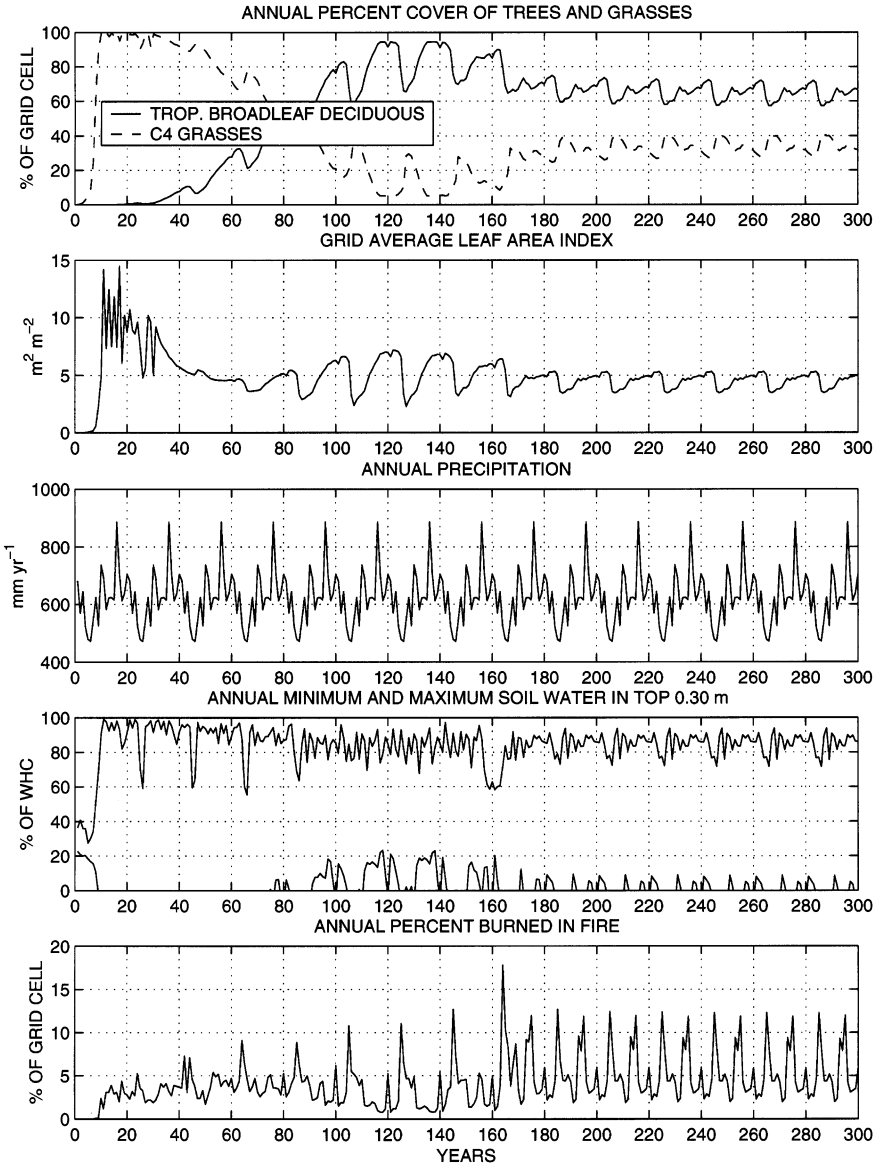

Fig. 15 LSM–DGVM vegetation dynamics over 300 years from initially bare ground for a grid cell in African savanna (13.5°N, 7.5°W). Percent cover is the annual extent of plant functional types in the grid cell. The leaf area index is the maximum attained each year. Annual precipitation, soil water in the top 30 cm (as a percent of water-holding capacity), and percent of the grid cell burned annually are also shown.

LSM–DGVM, this is manifested in the way in which interannual precipitation variability maintains a grass–tree mixture. Simulations that use a perpetually dry (1984, annual precipitation 472 mm), average (1986, annual precipitation 624 mm), or wet (1994, annual precipitation 887 mm) year give vegetation dominated by either grasses (dry, average) or trees (wet) depending on precipitation (not shown). This is consistent with the coupled climate–vegetation model results showing two stable regimes (wet–forest, dry–desert) in West Africa (Wang & Eltahir, 2000) and that interannual variability in precipitation contributes to the maintenance of African savanna (Zeng & Neelin, 2000).

Conclusions

These results show that simple ecological rules produce a realistic simulation of biogeography, net primary production, and vegetation dynamics. Sitch *et al*. (2003) show similar results for LPJ. This success is achieved without explicit representation of individual plants, age- or size-structure, gap dynamics, and the mosaic

pattern of landscapes – principles that have dominated forest dynamics theory and models for 30 years (Bormann & Likens, 1979; Shugart, 1984, 1998, 2000). Instead, each plant functional type patch is treated as a uniform dynamic unit. Gap dynamics is implicit. It occurs not at the scale of an individual, but rather in bulk parameterizations, in which establishment is limited to openings in the canopy and competition for space favors plant functional types with high leaf area. Moreover, the model distinguishes processes affecting the average individual (e.g., allometry) from processes affecting population density (e.g., mortality, establishment). A comparison of an individual plant model of vegetation dynamics and LPJ shows that the LPJ approach is successful, except in mixtures of deciduous and evergreen trees and where water stress favors grasses over trees (Smith *et al*., 2001).

The current definition of plant functional types is based on physiological and morphological traits along with climatic preferences in a manner similar to that proposed by Running *et al*. (1995) and Nemani & Running (1996). The distinction between annual or perennial, evergreen or deciduous, broadleaf or needleleaf, and woody or nonwoody is useful because these characteristics are observable by remote sensing and are key determinants of stomatal conductance, photosynthesis, and allocation. This physiological and morphological definition of plant functional types must be reconciled with an understanding of plant responses to disturbance, which is so critical to modeling vegetation dynamics. Ecologists have long characterized plants by life-history characteristics related to disturbance: r and K strategies (MacArthur & Wilson, 1967; Gadgil & Solbrig, 1972); early and late succession (Bazzaz, 1979; Huston & Smith, 1987); exploitive and conservative (Bormann & Likens, 1979); ruderal, stress tolerant, and competitive (Grime, 1979, 1993); vital attributes (Noble & Slayter, 1980); and gap and nongap species (Shugart, 1984, 1998). In many cases, these correlate with morphological and physiological traits. In the boreal forest succession (Fig. 10), the distinction between broadleaf deciduous and needleleaf evergreen also captures important differences in longevity, which drives stand dynamics. However, the tropical rainforest succession (Fig. 14), with only one broadleaf evergreen plant functional type, does not capture the observed succession from pioneer to climax species driven by gap dynamics (Richards, 1979; Ewel, 1983; Whitmore, 1990).

Smith *et al*. (2001) used a version of LPJ in which they distinguished shade-tolerant and -intolerant broadleaf deciduous trees. The shade-intolerant tree had faster growth, shorter longevity, higher sapling establishment, and needed more light for establishment than did the shade-tolerant tree. The model reproduced the classical successional series in which herbaceous ruderal species are replaced first by fast-growing, light-demanding pioneer species that give way to shade-tolerant species. Future work must determine the critical aspects of succession and plant life histories necessary to represent vegetation as a climate feedback.

Acknowledgements

This work was supported in part by the NASA Land Cover Land Use Change program through Grant W-19,735. The National Center for Atmospheric Research is sponsored by the National Science Foundation.

References

Aber JD (1979) Foliage-height profiles and succession in northern hardwood forests. *Ecology*, **60**, 18–23.

Bazzaz FA (1979) The physiological ecology of plant succession. *Annual Review of Ecology and Systematics*, **10**, 351–371.

Betts RA (2000) Offset of the potential carbon sink from boreal forestation by decreases in surface albedo. *Nature*, **408**, 187–190.

Blackmon M, Boville B, Bryan F *et al*. (2001) The community climate system model. *Bulletin of the American Meteorological Society*, **82**, 2357–2376.

Bliss LC (2000) Arctic tundra and polar desert biome. In: *North American Terrestrial Vegetation* 2nd edn (eds Barbour MG, Billings WD), pp. 1–40. Cambridge University Press, Cambridge.

Bliss LC, Cantlon JE (1957) Succession on river alluvium in northern Alaska. *American Midland Naturalist*, **58**, 452–469.

Bonan GB (1989) Environmental factors and ecological processes controlling vegetation patterns in boreal forests. *Landscape Ecology*, **3**, 111–130.

Bonan GB (1990a) Carbon and nitrogen cycling in North American boreal forests. I. Litter quality and soil thermal effects in interior Alaska. *Biogeochemistry*, **10**, 1–28.

Bonan GB (1990b) Carbon and nitrogen cycling in North American boreal forests. II. Biogeographic patterns. *Canadian Journal of Forest Research*, **20**, 1077–1088.

Bonan GB (1995) Land–atmosphere CO_2 exchange simulated by a land surface process model coupled to an atmospheric general circulation model. *Journal of Geophysical Research*, **100D**, 2817–2831.

Bonan GB (1996) *A land surface model (LSM version 1.0) for ecological, hydrological, and atmospheric studies: technical description and user's guide*, NCAR Technical Note NCAR/TN-417 + STR. National Center for Atmospheric Research, Boulder.

Bonan GB (1998) The land surface climatology of the NCAR land surface model coupled to the NCAR Community Climate Model. *Journal of Climate*, **11**, 1307–1326.

Bonan GB, Van Cleve K (1992) Soil temperature, nitrogen mineralization, and carbon source–sink relationships in boreal forests. *Canadian Journal of Forest Research*, **22**, 629–639.

Bonan GB, Pollard D, Thompson SL (1992) Effects of boreal forest vegetation on global climate. *Nature*, **359**, 716–718.

Bonan GB, Levis S, Kergoat L *et al*. (2002a) Landscapes as patches of plant functional types: an integrating concept for climate and ecosystem models. *Global Biogeochemical Cycles*, **16**, 1021, doi:10.1029/2000GB001360..

Bonan GB, Oleson KW, Vertenstein M *et al*. (2002b) The land surface climatology of the Community Land Model coupled to the NCAR Community Climate Model. *Journal of Climate*, **15**, 3123–3149.

Bormann FH, Likens GE (1979) *Pattern and Process in a Forested Ecosystem*. Springer-Verlag, New York.

Bormann FH, Siccama TG, Likens GE *et al*. (1970) The Hubbard Brook Ecosystem Study: composition and dynamics of the tree stratum. *Ecological Monographs*, **40**, 373–388.

Braconnot P, Joussaume S, deNoblet N *et al*. (2000) Mid-Holocene and Last Glacial Maximum African monsoon changes as simulated within the Paleoclimate Modelling Intercomparison Project. *Global and Planetary Change*, **26**, 51–66.

Brunig EF (1983) Vegetation structure and growth. In: *Tropical Rain Forest Ecosystems (Ecosystems of the World 14A)* (ed. Golley FB), pp. 49–75. Elsevier, Amsterdam.

Chalita S, LeTreut H (1994) The albedo of temperate and boreal forest and the Northern Hemisphere climate: a sensitivity experiment using the LMD GCM. *Climate Dynamics*, **10**, 231–240.

Chapin FS III, Chapin MC (1980) Revegetation of an Arctic disturbed site by native tundra species. *Journal of Applied Ecology*, **17**, 449–456.

Claussen M (1994) On coupling global biome models with climate models. *Climate Research*, **4**, 203–221.

Claussen M (1997) Modeling bio-geophysical feedback in the African and Indian monsoon region. *Climate Dynamics*, **13**, 247–257.

Claussen M (1998) On multiple solutions of the atmosphere-vegetation system in present-day climate. *Global Change Biology*, **4**, 549–559.

Claussen M, Gayler V (1997) The greening of the Sahara during the mid-Holocene: results of an interactive atmosphere-biome model. *Global Ecology and Biogeography Letters*, **6**, 369–377.

Claussen M, Brovkin V, Ganopolski A *et al*. (1998) Modelling global terrestrial vegetation-climate interaction. *Philosophical Transactions of the Royal Society of London*, **353B**, 53–63.

Claussen M, Brovkin V, Ganopolski A (2001) Biogeophysical versus biogeochemical feedbacks of large-scale land cover change. *Geophysical Research Letters*, **28**, 1011–1014.

Collatz GJ, Ball JT, Grivet C *et al*. (1991) Physiological and environmental regulation of stomatal conductance, photosynthesis and transpiration: a model that includes a laminar boundary layer. *Agricultural and Forest Meteorology*, **54**, 107–136.

Collatz GJ, Ribas-Carbo M, Berry JA (1992) Coupled photosynthesis-stomatal conductance model for leaves of C_4 plants. *Australian Journal of Plant Physiology*, **19**, 519–538.

Cox PM, Betts RA, Jones CD, Spall SA, Totterdell IJ (2000) Acceleration of global warming due to carbon-cycle feedbacks in a coupled climate model. *Nature*, **408**, 184–187.

Craig SG, Holmén KJ, Bonan GB *et al*. (1998) Atmospheric CO_2 simulated by the National Center for Atmospheric Research Community Climate Model 1. Mean fields and seasonal cycles. *Journal of Geophysical Research*, **103D**, 13213–13235.

Cramer W, Kicklighter DW, Bondeau A *et al*. (1999) Comparing global models of terrestrial net primary productivity (NPP): overview and key results. *Global Change Biology*, **5**, 1–15.

Cramer W, Bondeau A, Woodward FI *et al*. (2001) Global response of terrestrial ecosystem structure and function to CO_2 and climate change: results from six dynamic global vegetation models. *Global Change Biology*, **7**, 357–373.

Crowley TJ, Baum SK (1997) Effect of vegetation on an ice-age climate model simulation. *Journal of Geophysical Research*, **102D**, 16463–16480.

Delcourt HR, Delcourt PA (2000) Eastern deciduous forests. In: *North American Terrestrial Vegetation* 2nd edn (eds Barbour MG, Billings WD), pp. 357–395. Cambridge University Press, Cambridge.

de Noblet NI, Prentice IC, Joussaume S *et al*. (1996) Possible role of atmosphere-biosphere interactions in triggering the last glaciation. *Geophysical Research Letters*, **23**, 3191–3194.

de Noblet-Ducoudré N, Claussen M, Prentice C (2000) Mid-Holocene greening of the Sahara: first results of the GAIM 6000 year BP experiment with two asynchronously coupled atmosphere/biome models. *Climate Dynamics*, **16**, 643–659.

Doherty R, Kutzbach J, Foley J *et al*. (2000) Fully coupled climate/dynamical vegetation model simulations over Northern Africa during the mid-Holocene. *Climate Dynamics*, **16**, 561–573.

Douville H, Royer J-F (1996) Influence of the temperate and boreal forests on the Northern Hemisphere climate in the Météo-France climate model. *Climate Dynamics*, **13**, 57–74.

Ewel J (1983) Succession. In: *Tropical Rain Forest Ecosystems (Ecosystems of the World 14A)* (ed Golley FB), pp. 217–223. Elsevier, Amsterdam.

Farquhar GD, von Caemmerer S, Berry JA (1980) A biochemical model of photosynthetic CO_2 assimilation in leaves of C_3 species. *Planta*, **149**, 78–90.

Fetcher N, Beatty TF, Mullinax B *et al*. (1984) Changes in Arctic tussock tundra thirteen years after fire. *Ecology*, **65**, 1332–1333.

Foley JA, Kutzbach JE, Coe MT *et al*. (1994) Feedbacks between climate and boreal forests during the Holocene epoch. *Nature*, **371**, 52–54.

Foley JA, Prentice IC, Ramankutty N *et al*. (1996) An integrated biosphere model of land surface processes, terrestrial carbon balance, and vegetation dynamics. *Global Biogeochemical Cycles*, **10**, 603–628.

Foley JA, Levis S, Prentice IC *et al*. (1998) Coupling dynamic models of climate and vegetation. *Global Change Biology*, **4**, 561–579.

Gadgil M, Solbrig OT (1972) The concept of r- and K-selection: evidence from wild flowers and some theoretical considerations. *American Naturalist*, **106**, 14–31.

Gallimore RG, Kutzbach JE (1996) Role of orbitally induced changes in tundra area in the onset of glaciation. *Nature*, **381**, 503–505.

Golley FB (1983) The abundance of energy and chemical elements. In: *Tropical Rain Forest Ecosystems (Ecosystems of*

the World 14A) (ed Golley FB), pp. 101–115. Elsevier, Amsterdam.

Gower ST, Vogel JG, Norman JM *et al*. (1997) Carbon distribution and aboveground net primary production in aspen, jack pine, and black spruce stands in Saskatchewan and Manitoba, Canada. *Journal of Geophysical Research*, **102D**, 29029–29041.

Grime JP (1979) *Plant Strategies and Vegetation Processes*. Wiley, Chichester.

Grime JP (1993) Vegetation functional classification systems as approaches to predicting and quantifying global vegetation change. In: *Vegetation Dynamics and Global Change* (eds Solomon AM, Shugart HH), pp. 293–305. Chapman & Hall, New York.

Henderson-Sellers A (1993) Continental vegetation as a dynamic component of a global climate model: a preliminary assessment. *Climatic Change*, **23**, 337–377.

Hoelzmann P, Jolly D, Harrison SP *et al*. (1998) Mid-Holocene land-surface conditions in northern Africa and the Arabian peninsula: a data set for the analysis of biogeophysical feedbacks in the climate system. *Global Biogeochemical Cycles*, **12**, 35–51.

Huston M, Smith T (1987) Plant succession: life history and competition. *American Naturalist*, **130**, 168–198.

Jolly D, Harrison SP, Damnati B *et al*. (1998a) Simulated climate and biomes of Africa during the late Quaternary: comparison with pollen and lake status data. *Quaternary Science Reviews*, **17**, 629–657.

Jolly D, Prentice IC, Bonnefille R (1998b) Biome reconstruction from pollen and plant macrofossil data for Africa and the Arabian peninsula at 0 and 6000 years. *Journal of Biogeography*, **25**, 1007–1027.

Kubatzki C, Claussen M (1998) Simulation of the global biogeophysical interactions during the Last Glacial Maximum. *Climate Dynamics*, **14**, 461–471.

Kucharik CJ, Foley JA, Delire C *et al*. (2000) Testing the performance of a dynamic global ecosystem model: water balance, carbon balance, and vegetation structure. *Global Biogeochemical Cycles*, **14**, 795–825.

Kutzbach JE, Otto-Bliesner BL (1982) The sensitivity of the African–Asian monsoonal climate to orbital parameter changes for 9000 years BP in a low-resolution general circulation model. *Journal of the Atmospheric Sciences*, **39**, 1177–1188.

Kutzbach J, Bonan G, Foley J *et al*. (1996) Vegetation and soil feedbacks on the response of the African monsoon to orbital forcing in the early to middle Holocene. *Nature*, **384**, 623–626.

Levis S, Foley JA, Pollard D (1999) CO_2, climate, and vegetation feedbacks at the Last Glacial Maximum. *Journal of Geophysical Research*, **104D**, 31191–31198.

Levis S, Foley JA, Pollard D (2000) Large-scale vegetation feedbacks on a doubled CO_2 climate. *Journal of Climate*, **13**, 1313–1325.

Likens GE, Bormann FH, Pierce RS, *et al* (1977) *Biogeochemistry of a Forested Ecosystem*. Springer-Verlag, New York.

MacArthur RH, Wilson EO (1967) *The Theory of Island Biogeography*. Princeton University Press, Princeton.

Marks PL (1974) The role of pin cherry (*Prunus pensylvanica* L) in the maintenance of stability in northern hardwood ecosystems. *Ecological Monographs*, **44**, 73–88.

McGuire AD, Sitch S, Clein JS *et al*. (2001) Carbon balance of the terrestrial biosphere in the twentieth century: analyses of CO_2, climate and land use effects with four process-based ecosystem models. *Global Biogeochemical Cycles*, **15**, 183–206.

Nemani R, Running SW (1996) Implementation of a hierarchical global vegetation classification in ecosystem function models. *Journal of Vegetation Science*, **7**, 337–346.

Noble IR, Slayter RO (1980) The use of vital attributes to predict successional changes in plant communities subject to recurrent disturbances. *Vegetatio*, **43**, 5–21.

Prentice IC, Jolly DBIOME 6000 participants (2000) Mid-Holocene and glacial-maximum vegetation geography of the northern continents and Africa. *Journal of Biogeography*, **27**, 507–519.

Racine CH, Johnson LA, Viereck LA (1987) Patterns of vegetation recovery after tundra fires in northwestern Alaska, USA. *Arctic and Alpine Research*, **19**, 461–469.

Ramankutty N, Foley JA (1999) Estimating historical changes in global land cover: croplands from to 1700 to 1992. *Global Biogeochemical Cycles*, **13**, 997–1027.

Richards PW (1979) *The Tropical Rain Forest*. Cambridge University Press, Cambridge.

Ruess RW, Van Cleve K, Yarie J *et al*. (1996) Contributions of fine root production and turnover to the carbon and nitrogen cycling in taiga forests of the Alaskan interior. *Canadian Journal of Forest Research*, **26**, 1326–1336.

Running SW, Loveland TR, Pierce LL *et al*. (1995) A remote sensing based vegetation classification logic for global land cover analysis. *Remote Sensing of Environment*, **51**, 39–48.

Schlesinger WH (1997) *Biogeochemistry: An Analysis of Global Change* 2nd edn. Academic Press, San Diego.

Scholes RJ, Walker BH (1993) *An African Savanna: Synthesis of the Nylsvley Study*. Cambridge University Press, Cambridge.

Sellers PJ, Dickinson RE, Randall DA *et al*. (1997) Modeling the exchanges of energy, water, and carbon between continents and the atmosphere. *Science*, **275**, 502–509.

Shugart HH (1984) *A Theory of Forest Dynamics: The Ecological Implications of Forest Succession Models*. Springer-Verlag, New York.

Shugart HH (1998) *Terrestrial Ecosystems in Changing Environments*. Cambridge University Press, Cambridge.

Shugart HH (2000) Importance of structure in the longer-term dynamics of landscapes. *Journal of Geophysical Research*, **105D**, 20065–20075.

Sims PL, Risser PG (2000) Grasslands. In: *North American Terrestrial Vegetation* 2nd edn (eds Barbour MG, Billings WD), pp. 323–356. Cambridge University Press, Cambridge.

Sitch S, Smith B, Prentice IC *et al*. (2003) Evaluation of ecosystem dynamics, plant geography and terrestrial carbon cycling in the LPJ dynamic global vegetation model. *Global Change Biology*, **9**, 161–185.

Smith B, Prentice IC, Sykes MT (2001) Representation of vegetation dynamics in the modelling of terrestrial ecosystems: comparing two contrasting approaches within European climate space. *Global Ecology and Biogeography*, **10**, 621–637.

Steele SJ, Gower ST, Vogel JG *et al*. (1997) Root mass, net primary production and turnover in aspen, jack pine and black spruce

forests in Saskatchewan and Manitoba, Canada. *Tree Physiology*, **17**, 577–587.

Texier D, de Noblet N, Harrison SP *et al*. (1997) Quantifying the role of biosphere-atmosphere feedbacks in climate change: coupled model simulations for years BP and comparison with palaeodata for northern Eurasia and northern Africa. *Climate Dynamics*, **13**, 865–882.

Thomas G, Rowntree PR (1992) The boreal forests and climate. *Quarterly Journal of the Royal Meteorological Society*, **118**, 469–497.

Thonicke K, Venevsky S, Sitch S *et al*. (2001) The role of fire disturbance for global vegetation dynamics: coupling fire into a dynamic global vegetation model. *Global Ecology and Biogeography*, **10**, 661–677.

Van Cleve K, Dyrness CT, Viereck LA *et al*. (1983a) Taiga ecosystems in interior Alaska. *BioScience*, **33**, 39–44.

Van Cleve K, Oliver L, Schlentner R *et al*. (1983b) Productivity and nutrient cycling in taiga forest ecosystems. *Canadian Journal of Forest Research*, **13**, 747–766.

Van Cleve K, Chapin FS, Flanagan PW, *et al* (1986) *Forest Ecosystems in the Alaskan Taiga*. Springer-Verlag, New York.

Van Cleve K, Chapin FS III, Dyrness CT *et al*. (1991) Element cycling in taiga forests: state-factor control. *BioScience*, **41**, 78–88.

Walker BH (1981) Is succession a viable concept in African savanna ecosystems? In: *Forest Succession: Concepts and Application* (eds West DC, Shugart HH, Botkin DB), pp. 431–447. Springer-Verlag, New York.

Wang G, Eltahir EAB (2000) Biosphere-atmosphere interactions over West Africa. II: multiple climate equilibria. *Quarterly Journal of the Royal Meteorological Society*, **126**, 1261–1280.

Wein RW, Bliss LC (1973) Changes in Arctic *Eriophorum* tussock communities following fire. *Ecology*, **54**, 845–852.

Whitmore TC (1990) *An Introduction to Tropical Rain Forests*. Oxford University Press, Oxford.

Whittaker RH, Bormann FH, Likens GE *et al*. (1974) The Hubbard Brook Ecosystem Study: forest biomass and production. *Ecological Monographs*, **44**, 233–252.

Wullschleger SD (1993) Biochemical limitations to carbon assimilation in C_3 plants – a retrospective analysis of the A/C_i curves from 109 species. *Journal of Experimental Botany*, **44**, 907–920.

Zeng N, Neelin JD (2000) The role of vegetation-climate interaction and interannual variability in shaping the African savanna. *Journal of Climate*, **13**, 2665–2670.